Journal of Medicinal Chemistry

Article

Cite This: J. Med. Chem. 2019, 62, 11383−11398

pubs.acs.org/jmc

Kinetic Optimization of Lysine-Targeting Covalent Inhibitors of HSP72

Jonathan Pettinger, Michael Carter, Keith Jones, and Matthew D. Cheeseman*

Cancer Research UK Cancer Therapeutics Unit, The Institute of Cancer Research, London SW7 3RP, United Kingdom

Supporting Information

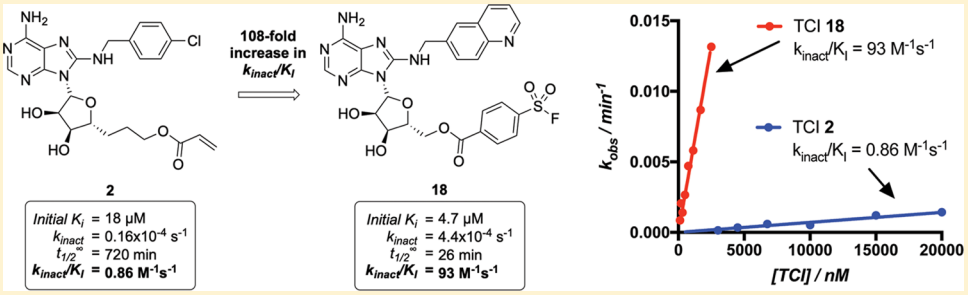

ABSTRACT: The covalent inhibition mechanism of action, which overcomes competition with high-affinity, high-abundance substrates of challenging protein targets, can deliver effective chemical probes and drugs. The success of this strategy has centered on exposed cysteine residues as nucleophiles but the low abundance of cysteine in the proteome has limited its application. We have recently reported our discovery that lysine-56 in the difficult-to-drug target HSP72 could form a covalent bond with a small-molecule inhibitor. We now disclose the optimization of these targeted covalent inhibitors using rational design. Essential to our optimization was the development of a new covalent fluorescence polarization assay, which allows for the direct measurement of the key kinetic parameter in covalent inhibitor design, k_{inact}/K_I, extrapolation of the underlying parameters, k_{inact} and K_i, and direct comparison to reversible analogues. Using our approach, we demonstrate a >100-fold enhancement in covalent efficiency and key learnings in lysine-selective electrophile optimization.

INTRODUCTION

Despite many of our most important drugs utilizing irreversible covalent inhibition of an enzyme,[1] concerns relating to idiosyncratic toxicity led to the near-exclusion of this mechanism of action (MOA) from drug discovery programs.[2] The recent renaissance in covalent inhibitors is in large part due to their inherent advantage over reversible counterparts for antagonising proteins that have high-affinity, high-abundance natural substrates.[3] While the previous generation of irreversible inhibitor drugs were discovered by serendipity or were natural products, the rational design strategy for modern targeted covalent inhibitors (TCIs) focuses on exploiting high-resolution small-molecule/protein X-ray crystal structures of high-affinity reversible ligands to target active site, solvent-exposed cysteine residues with sparingly reactive electrophiles.[4] Unfortunately, the rarity of cysteine in the proteome has limited its application,[5] leading to an increased interest in targeting other potentially nucleophilic residues.[6−8]

Depending on the length of exposure and the concentration, TCIs utilize both reversible and irreversible occupancy of a protein (Figure 1B).[9] Defining a TCI only via an IC_{50} value can be limiting for rational design, as the inhibitor (I) will inevitably appear more potent with increasing preincubation time. TCIs typically react via a two-step MOA (Figure 1A), initially binding to the protein (E) in a reversible manner to generate a noncovalent complex (EI). The occupancy of the reversible complex is determined by the free concentration of the TCI and the equilibrium constant K_i. The reversible complex can then undergo covalent bond formation as determined by the first-order rate constant k_{inact}, to give the covalent complex (E-I). These fundamental parameters describe the efficiency of the TCI but cannot be determined directly from assay data.

TCI activity is described by an equation analogous to the Michaelis−Menten equation. When normalized for protein concentration, the rate of covalent bond formation can be quantified by the pseudo-first-order rate constant, k_{obs} (Figure 1C). The reversible binding event, k_{obs} is not a true constant, as its value is dependent on the concentration of the TCI. At TCI concentrations approaching binding-site saturation, k_{obs} tends to the constant, k_{inact}, equivalent to the half-life of the reaction at a theoretical infinite concentration ($t_{1/2}^{inf}$).[10] [I] at $k_{inact}/2$ determines the pseudo-equilibrium constant K_I, equivalent to K_m when describing enzyme substrates. The true reversible equilibrium constant for the process, K_i, is often used interchangeably with K_I, but this is only a fair assumption when $k_{inact} \ll k_{off}$[11] and may not be true for tight reversible binding TCIs. At concentrations much lower than K_I, the response of k_{obs} to changing TCI concentration becomes linear. The gradient of this relationship gives the second-order rate

Received: October 16, 2019
Published: November 14, 2019

DOI: 10.1021/acs.jmedchem.9b01709
J. Med. Chem. 2019, 62, 11383−11398

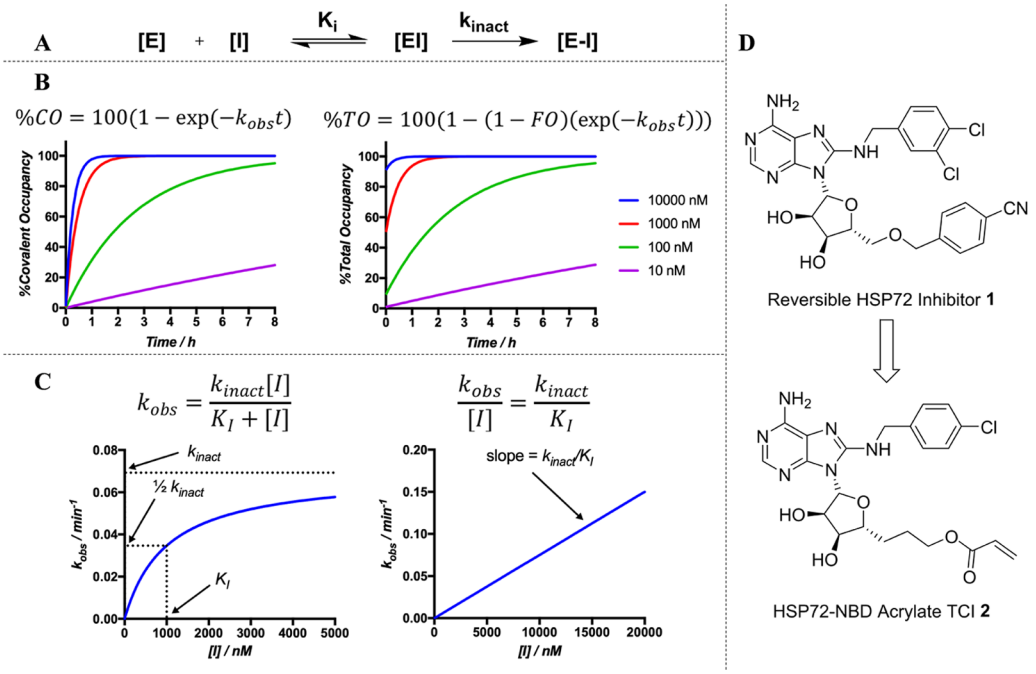

Figure 1. Simulated data describing the MOA and kinetic parameters used to quantify the activity of TCIs. (A) TCI two-step binding mechanism. (B) The two components of TCI MOA, both reversible and covalent occupancy, contribute to the total target occupancy at a given concentration and time. Left = covalent occupancy (%CO) and right = total occupancy (%TO), both simulated using K_I = 1 μM and k_{inact} = 0.069 min^{-1}. FO = fraction reversible occupancy (see Supporting Information for derivation). (C) Determination of the essential second-order rate constant k_{inact}/K_I from the concentration-dependent k_{obs} pseudo-first-order rate constant. Left = example where K_I < [I] so k_{inact} and K_I can be deconvoluted. Right = example where $K_I \gg$ [I] so the individual kinetic parameters cannot be distinguished. (D) Nucleoside-derived reversible **1** and covalent inhibitor **2** of HSP72.

constant k_{inact}/K_I, which is the key kinetic parameter that describes the efficiency of the reaction, and its optimization is the primary goal of any TCI discovery effort toward a chemical probe (Figure 1C).

Analysis of the k_{inact}/K_I parameter clearly demonstrates that there are two strategies for TCI optimization: first, through the reduction of K_I by increasing the reversible affinity of the ligand for the target protein, and second by increasing k_{inact}. The optimization of k_{inact} differs from simply increasing the intrinsic reactivity of the electrophile, as this would likely lead to a greater off-target activity; instead, k_{inact} optimization focuses on the particular environment within the protein-binding site compared to bulk aqueous solvent.[12] The effect of solvent dielectric constant, proximal residues, perturbed pK_a, and the tightly controlled bond angles and distances resulting from the reversible binding of the ligand can lead to a dramatically enhanced rate of covalent bond formation and high selectivity. This effect of binding-site rate enhancement has led to effective, highly selective, and successful TCI design of KRAS G12C inhibitors, which display a very weak reversible affinity but exploit extremely high k_{inact} values with sparingly low intrinsic reactivity electrophiles, resulting in k_{inact}/K_I values suitable for in vivo efficacy.[13,14]

Heat shock 70 kDa protein 1 (HSP72) is a member of the HSP70 family of molecular chaperones. It is an ATPase that binds misfolded proteins, stabilizing the cellular environment and allowing the cell to return to homeostasis.[15] HSP72 is induced in an HSF1-dependent manner when the cell is undergoing stress and is overexpressed in several cancer cell types.[16] This overexpression is correlated with metastasis, poor prognosis, and resistance to chemotherapy in patients.[17] Because of the clear role of HSP72 in cancer, it has become an important target in drug discovery, but despite considerable research effort, there is currently no potent, selective, cellularly active chemical probe to study the function of HSP72 in cancer cells.

The nucleotide-binding domain (NBD) of HSP72 (HSP72-NBD) can be reversibly targeted with a series of *bis*-aryl nucleoside-derived inhibitors (Figure 1D), which display a very high apparent affinity in biochemical assays but suffer a steep dropoff in activity in cancer cells.[18] We hypothesized that the poor cellular activity of this chemotype was due to competition with the high-affinity (K_M for ATP = ~1 μM), high-abundance (~5 mM)[19] substrate of HSP72, ATP. We have recently reported the discovery that lysine-56 can be selectivity targeted with an acrylate-derived TCI **2** (Figure 1D).[20] Targeting lysine residues with TCIs presents a number of unique challenges and is still in its infancy,[21] but the greater prevalence of lysine in the proteome[22] could result in more wide-ranging applications of the irreversible inhibitor paradigm than has so far been possible through the rational targeting of cysteine.

As part of our continuing effort to develop strategies and techniques to discover lysine-targeting covalent ligands, we now report the disclosure of an HSP72 TCI, where our approach led to a 108-fold improvement in k_{inact}/K_I. Critical to the optimization was the development of a covalent fluorescence polarization (covalent FP) assay that can distinguish between the reversible and covalent components of target occupancy, allowing for a direct comparison between covalent and reversible analogues, which is essential for correct structure activity relationship (SAR) interpretation. The covalent FP-assay will be widely applicable to the optimization of TCIs of other nonenzymatic or poorly catalytic proteins.

DOI: 10.1021/acs.jmedchem.9b01709
J. Med. Chem. 2019, 62, 11383−11398

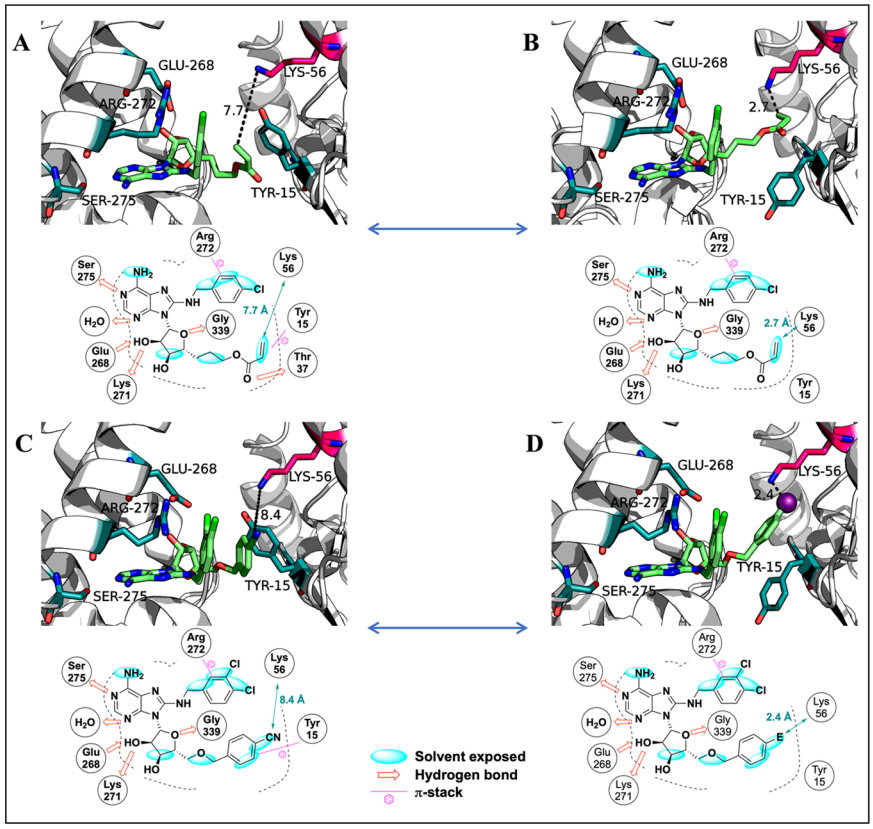

Figure 2. Analysis of Lys56-targeting TCI binding modes. The tertiary conformation of the protein is maintained in the previously described semiopen form in all structures and modeling. The polar interactions of the adenine-type base and ribose are maintained in each binding mode. All diagrams were adapted from analysis using MOE (2014.09) and PyMOL Molecular Graphics System, Version 2.0 Schrödinger, LLC. 2.2.3 A: Tyr15 up-conformation. The acrylate electrophile of **2** forms a π-stack interaction with Tyr15 and a hydrogen bond with Thr-37. In this reversible complex, the electrophile is too far from Lys56 to form a covalent bond (PDB: 5MKR). B: Tyr15 downconformation. Following rotation of Tyr15, rotation around the linker of **2** now positions the acrylate electrophile in close proximity to Lys56, suitable for covalent-bond formation in this precovalent complex. The acrylate moiety was not observed in the electron density due to flexibility, so was modeled to estimate distances (PDB: 5MKS). C: Binding mode of the high-affinity reversible HSP72 inhibitor **1** in the Tyr15 upconformation (PDB: 4IO8). D: Model of a putative binding mode for a high-affinity Lys56-targeting TCI. With Tyr15 in a downconformation, rotation of the benzylic ether positions a potential *para*-electrophile at an appropriate distance from Lys56 in a precovalent complex. E: Three-step MOA, TCI binds HSP72 to form the reversible complex (EI) before transition to the precovalent complex (EI*) that can result in the formation of the covalent bond and the irreversible complex (E-I).

RESULTS AND DISCUSSION

Analysis of the First-Generation Lysine-56 TCI Binding Mode and Optimization of K_i. Exploiting extensive mass spectrometry studies, single-point mutant proteins, and through the design of several key control compounds, we had previously demonstrated that our first-generation acrylate TCI **2** (Figure 1D) was both highly selective for lysine-56 and that an initial reversible binding step was critical to its MOA. However, the rate of reaction of **2** was very slow, requiring >24 h exposure, even at high concentrations, before the intact-protein mass spectrometry (**MS**) indicated complete formation of the covalent complex.[20] Therefore, our aim was to develop a strategy to optimize lysine-56-targeting TCIs of HSP72 toward a potentially cell active chemical probe.

To redesign the second-generation TCI with increased potency, we analyzed our two previously reported co-crystal structures of HSP72-NBD with acrylate TCI **2** reversibly bound.[20] These structures revealed two distinct binding modes and protein-residue conformations, which we hypothesized were both essential for the efficiency of the covalent inhibition MOA (Figure 2A,B).

In the putative reversible complex of acrylate TCI **2** (Figure 2A, PDB: 5MKR),[20] Tyr15 was in an upconformation, blocking any direct vector from the ligand to the nucleophilic Lys56. The electrophilic acrylate moiety formed an eclipsed conformation, resulting in a π-stack interaction with Tyr15 and a hydrogen bond to Thr37. In the putative precovalent complex (Figure 2B, PDB: 5MKS),[20] the electrophile was observed in an elongated conformation and with Tyr15 in a downconformation.[23,24] The conformational flip of Tyr15 allowed the acrylate moiety to position proximally to the Lys56 nucleophile, which is essential for covalent-bond formation. The hydrogen-bonding array of the 8-aminoadenosine-motif and the position of the lipophilic *p*-chlorophenyl substituent were maintained in both binding modes. From this analysis, we proposed that the MOA of an HSP72 TCI proceeds via a three-step mechanism (Figure 2E). First, the TCI binds HSP72 to give a reversible complex (EI) that would contribute to the reversible occupancy but could not lead directly to covalent occupancy. Transition of the reversible complex (EI) to the precovalent complex (EI*) would be essential for the formation of the covalent bond and the resulting irreversible complex (E-I). Optimization of the affinity

DOI: 10.1021/acs.jmedchem.9b01709
J. Med. Chem. 2019, 62, 11383−11398

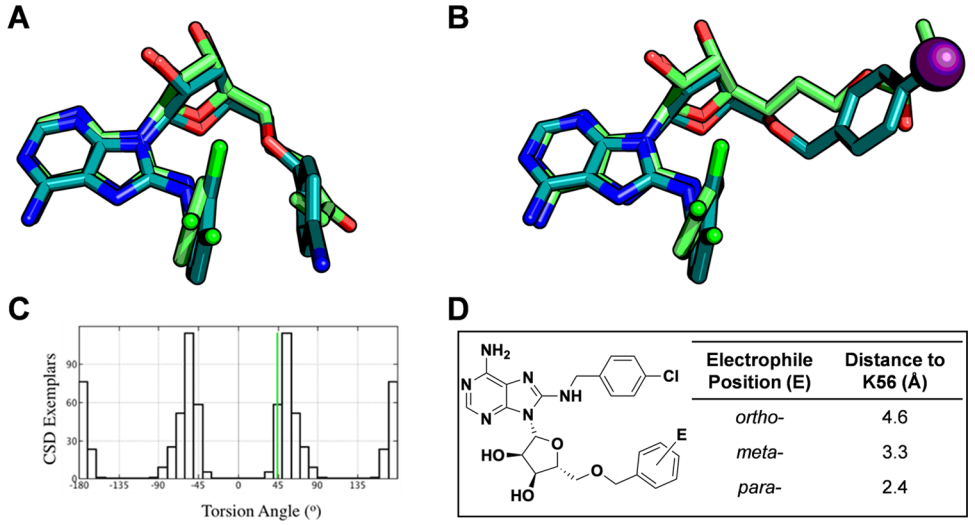

Figure 3. Conformation analysis of the proposed second-generation HSP72 TCI. A: Overlay of the acrylate TCI **2** (green) and the high-affinity reversible inhibitor **1** (cyan). B: Overlay of the acrylate TCI **2** (green) and the proposed conformation of the second-generation TCI (cyan) in the precovalent complex. The generic electrophile is represented as a purple sphere. C: Frequency distribution of torsional angles for 5′-*O*-adenosine derivatives observed in the CSD; the green line represents the desired torsional angle. D: At the desired torsional angle, the modeled distances to Lys56 from different ring positions.

Scheme 1. Synthesis of the Second-Generation Lysine-56-Targeting TCI[a]

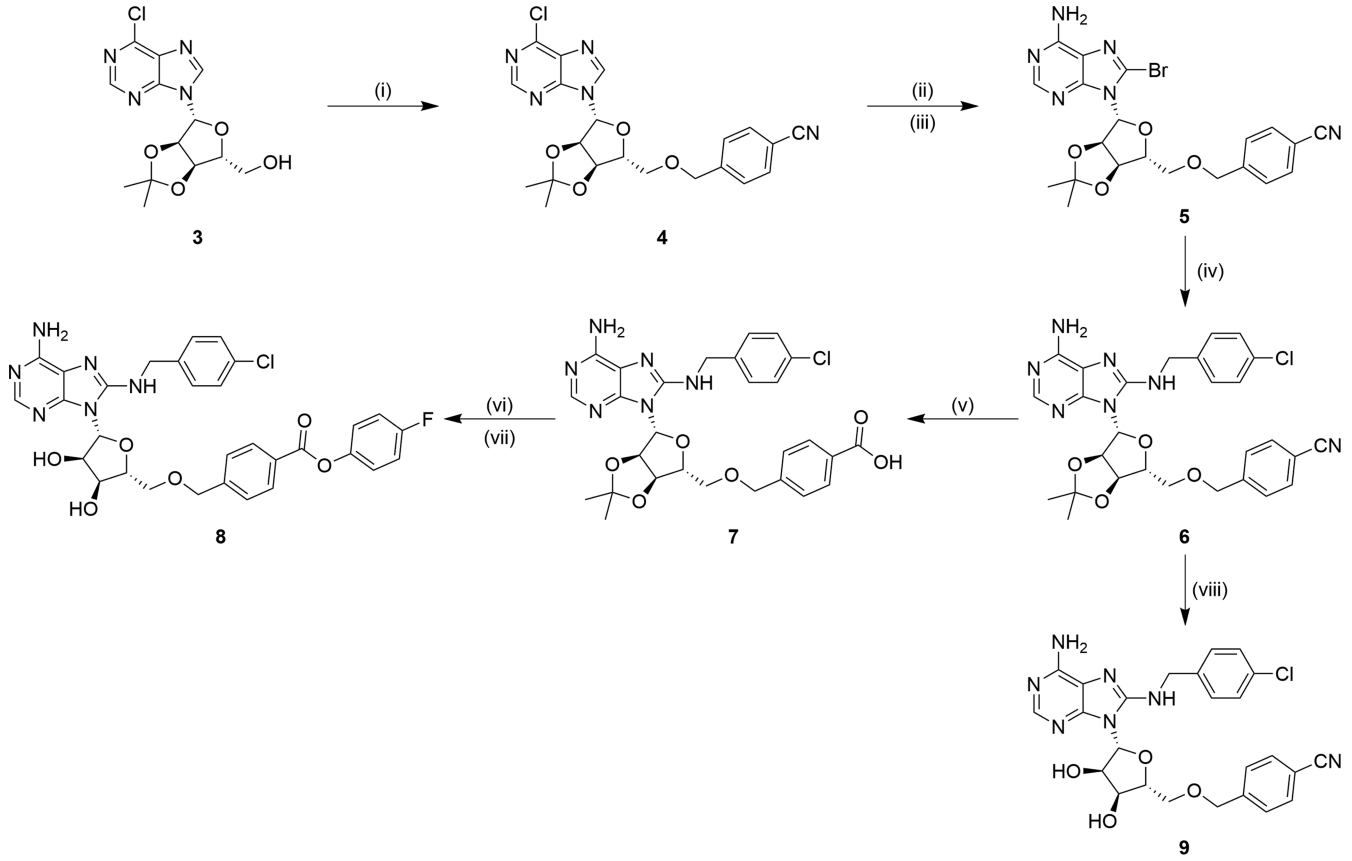

[a]Reagents and conditions: (i) 4-(bromomethyl) benzonitrile, NaH (60% in mineral oil), dimethylformamide (DMF), room temperature (RT), 1 h, 56%; (ii) 7 M NH_3/MeOH, 110 °C, MW, 2 h, 82%; (iii) Br_2, $K_2HPO_4 \cdot 3H_2O$, H_2O, 1,4-dioxane, RT, 1 h, 72%; (iv) 4-chlorobenzylamine, EtOH, 160 °C, MW, 1 h, 66%; (v) 2 M NaOH, EtOH, 100 °C 3 h, 58%; (vi) 4-fluorophenol, HATU, DIPEA, DMF, RT, 18 h, 47%; (vii) TFA/H_2O (5:2), RT, 0.5 h, 85%; (viii) 5:2 TFA/H_2O, RT, 0.5 h, 47%.

for the reversible complex would still result in increased potency of the covalent bond formation, although K_i would now describe a pseudo-equilibrium constant as a combination of the microscopic rate constants for the formation of the encounter complex and conformational switch, in a manner consistent with an induced fit binding MOA.[25] This would also

DOI: 10.1021/acs.jmedchem.9b01709
J. Med. Chem. 2019, 62, 11383−11398

Table 1. Kinetic and Affinity Analysis of Covalent and Noncovalent Inhibitors of HSP72[a–f]

Entry	Cd	Time (h)	[a]App. K_i (μM)	[b]k_{inact}/K_I ($M^{-1}s^{-1}$)	[c]k_{inact} (x10^{-4} s^{-1})	[d]$t_{1/2}^{inf}$ (min)	[d]Initial K_I (μM)
1	2	0.083	17	0.862±0.022	0.16	720	18
		19	7.2				
		46	3.7				
2	9	NA	<0.20				
3	8	0.083	2.5				
		2.0	2.0				
		24	1.4				
4	15	NA	3.5				
5	13	0.083	>200				
		1.0	>200				
		2.0	>200				
6	14	0.083	6.9	35±1.7	3.6	32	10
		1.0	0.52				
		2.0	0.25				
7	16	ND	ND	0.5±0.02	ND	ND	>600
8	17	ND	ND	3.3±0.03	3.7	31	110
		0.33	12				
		1.0	8.0				
9	18	0.083	3.3	93±2.9	4.4	26	4.7
		0.33	0.22				
		1.0	<0.20				

[a]All data were processed and analyzed using GraphPad Prism 7.04. All values are quoted to two significant figures. NA = not applicable, ND = not determined. [b]App. K_i = Apparent K_i. Each concentration represents n = 3 statistical repeats, arithmetic mean ± standard error of the mean (SEM). Each time course was generated from continuous measurements of each assay and assumes no significant TCI depletion. App. K_i values were calculated from the fitted IC_{50} curve using nonlinear regression (four parameters) using the method in ref 27 (see the Supporting Information). [c]Calculated using the method described in Figure 4. Each value represents the arithmetic mean ± SEM of n = 3 biological repeats. [d]Calculated from the respective k_{inact}/K_I and initial K_i values using the method described in Figure 4. [e]$t_{1/2}^{inf} = \ln 2/k_{inact}$. [f]Calculated from the IC_{50} curves using nonlinear regression (four parameters) using the method described in Figure 4.

assume that the conformational flexibility of Tyr15 is sufficient to allow transition to the precovalent complex and access the Lys56 nucleophile so that covalent bond formation is rate determining in k_{inact}.

To optimize the reversible affinity of our TCI, we aimed to exploit the high-affinity 5′-*O*-benzyl class of HSP72 inhibitors (Figure 2C). Analysis of the reversible complex (PDB: 4IO8)[26] of nitrile **1** (FP-Assay pK_i > 6.70, K_i = <0.20 μM, N = 3)[27,28] revealed that this ligand forms similar polar and lipophilic interactions in the 8-aminoadenosine- and *p*-chlorophenyl-regions of HSP72-NBD as our acrylate TCI **2**. Importantly, the 5′-*O*-benzyl substituent occupies the same pocket as the acrylate moiety, so we hypothesized that a benzyl group with an appropriately positioned electrophile could exploit both the high-affinity reversible complex and could transition to the precovalent complex (Figure 2D) in a similar putative three-

DOI: 10.1021/acs.jmedchem.9b01709
J. Med. Chem. 2019, 62, 11383−11398

Table 2. HSP72 TCI Analysis[a–d]

Entry	Cd	[a]App. K_i	[b]Intact Protein MS	[c]k_{inact}/K_I
1	**2**	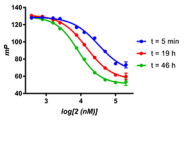	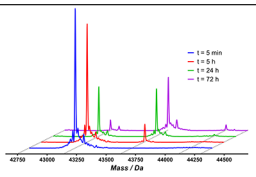	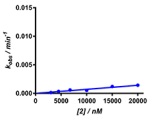
2	**8**	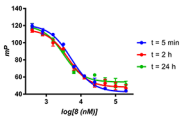	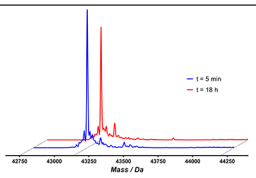	NA
3	**13**	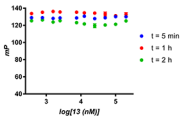	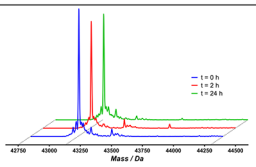	NA
4	**14**	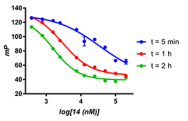	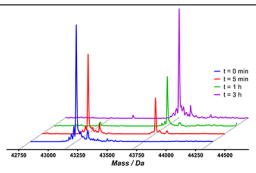	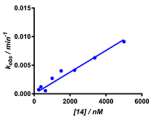
5	**16**	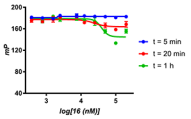	ND	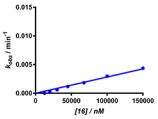
6	**17**	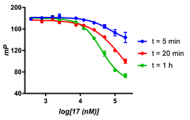	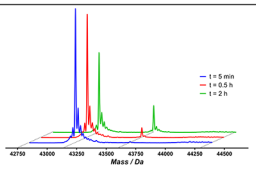	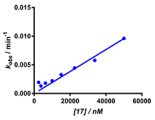
7	**18**	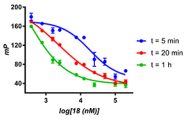	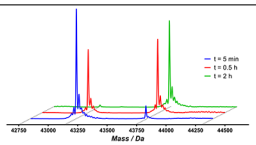	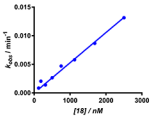

[a]All data were processed and analyzed using GraphPad Prism 7.04. [b]App. K_i = Apparent K_i. Each concentration represents $n = 3$ statistical repeats, arithmetic mean ± SEM. Each time course was generated from continuous measurements of each assay and assumes no significant TCI depletion. App. K_i values were calculated from the fitted IC_{50} curve using nonlinear regression (four parameters) using the method in ref 27 (see the Supporting Information). [c]Intact protein mass spectrometry. Entry 1: HSP72-NBD [2.3 μM] and TCI [200 μM] incubated for the time indicated. Entries 2–4: HSP72-NBD [2.0 μM] and TCI [20 μM] incubated for the time indicated. The MS of the resulting protein/TCI adducts were analyzed using Agilent MassHunter Qualitative B.06. [d]k_{inact}/K_I values calculated from the covalent FP-assay. The gradient of each slope was calculated from the linear regression, representative example of $N = 3$ independent biological repeats (see the Supporting Information for details).

step mechanism to our acrylate TCI **2**. To assess whether the proposed transition of the reversible to the precovalent complex was viable (Figure 3B), we carried out a rapid overlay of chemical structures (ROCS)[29] ligand-based analysis on the favorability of the linker torsional angles in this conformationally restricted structure, as this would be critical if we were to incorporate a 5′-benzylic substituent in our TCI design. Through alignment of the 5′-*O*-benzyl motif of **1** to the precovalent complex acrylate conformation of **2** and by comparison with known conformations of this chemotype in the Cambridge Structural Database (CSD)[30] (Figure 3C), it was demonstrated that a second-generation inhibitor could adopt an acceptable benzylic torsional angle, resulting in a viable conformation for covalent-bond formation. Finally, in this conformation, the *para*-position gave the shortest distance to Lys56 (Figure 3D), so an electrophile at this position was incorporated to complete our rational design hypothesis for the second-generation HSP72 TCI.

DOI: 10.1021/acs.jmedchem.9b01709
J. Med. Chem. 2019, 62, 11383–11398

Scheme 2. Synthesis of Third-Generation Aryl Sulfonyl Fluoride HSP72 TCIs[a]

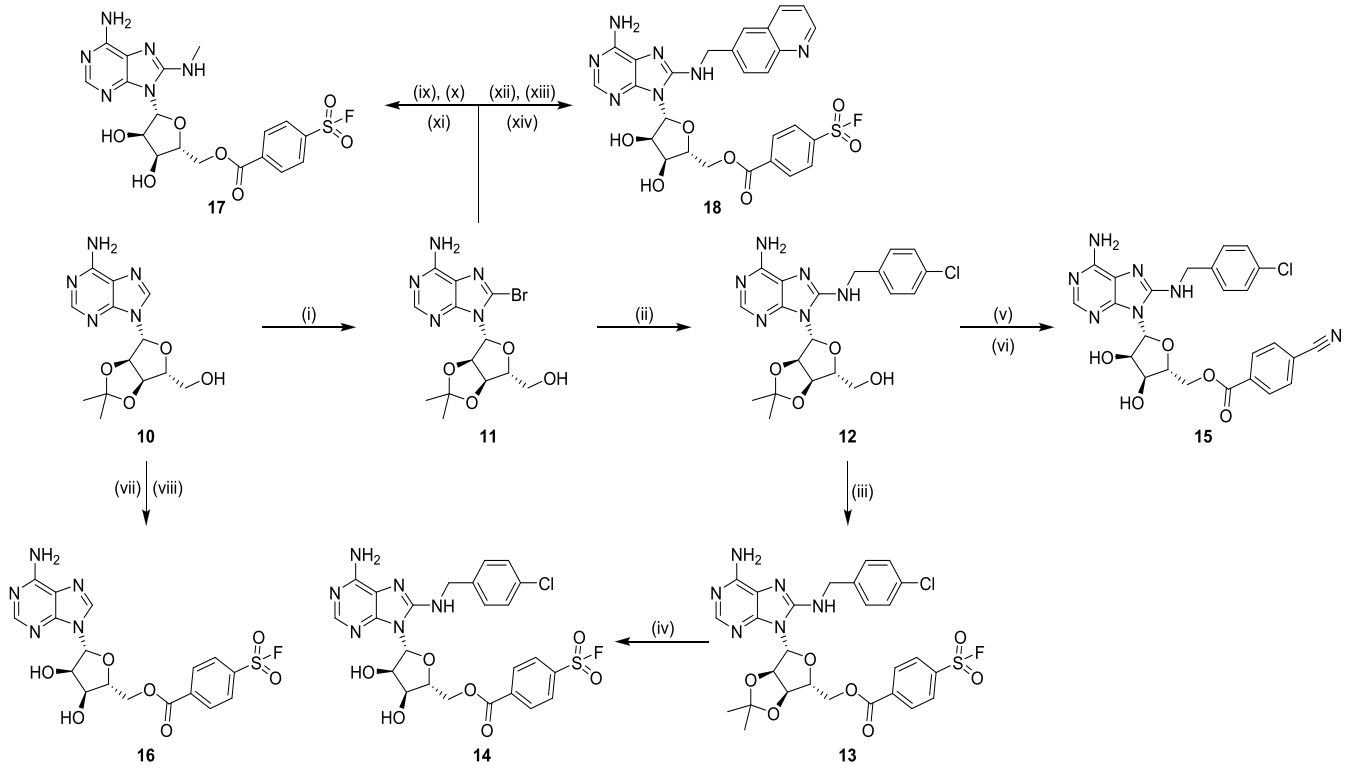

[a]Reagents and conditions: (i) Br_2, $K_2HPO_4 \cdot 3H_2O$, 1,4-dioxane, H_2O, RT, 0.5 h, 74%; (ii) 4-chlorobenzylamine, EtOH, 160 °C MW, 1 h, 97%; (iii) 4-(fluorosulfonyl)benzoyl chloride, Et_3N, DMF, 0 °C, 4 h; 56% (iv) 5:2 TFA/H_2O, RT, 0.5 h, 32%; (v) 4-cyanobenzoyl chloride, Et_3N, DMF, 0 °C, 3 h; (vi) 5:2 TFA/H_2O, RT, 0.5 h, 16% over two steps; (vii) 4-(fluorosulfonyl)benzoic acid, HBTU, Et_3N, DMF, RT, 2 h; 66%; (viii) 5:2 TFA/H_2O, RT, 0.5 h, 74%; (ix) 33% $MeNH_2$ in EtOH, 160 °C, MW, 1 h, 77%; (x) 4-(fluorosulfonyl)benzoic acid, HBTU, Et_3N, DMF, RT, 2 h; 35%; (xi) 5:2 TFA/H_2O, RT, 0.5 h, 40%; (xii) quinoline-6-yl methanamine, EtOH, 160 °C, MW, 2 h, 8%; (xiii) 4-(fluorosulfonyl)benzoic acid, HBTU, Et_3N, DMF, RT, 2 h; 40%; (xiv) 5:2 TFA/H_2O, RT, 0.5 h, 11%.

Selection and Synthesis of a Lysine-Targeting Warhead and Optimization of k_{inact}. Our first-generation TCI **2** utilized an acrylate warhead to form the covalent bond, which we hypothesized was suboptimal for targeting lysine residues in proteins. Lysine is a hard nucleophile and hence should display an enhanced rate of reaction with hard electrophiles, but few lysine-selective electrophiles have so far been described in the literature.[31] A recent study by Campos et al. successfully exploited activated phenolic esters as hard electrophiles to target the catalytic lysine of PI3Kδ.[32] To incorporate this concept into the design of our second-generation TCI, we developed a synthetic strategy that added an activated ester with a *p*-fluorophenol leaving group into the 5′-*para*-benzylic vector we had identified from our TCI MOA analysis.

The synthesis of the second-generation TCI began with benzylation of the 5′-hydroxyl of 2′,3′-acetonide-protected 6-chlororiboside **3** (Scheme 1). The order of addition is essential in this transformation to avoid oligomerization at the 6-chloro position; **3** was first treated with 4-(bromomethyl) benzonitrile, followed by exposure to NaH at 0 °C,[18] which gave the 5′-ether **4** in 56% yield. S_NAr displacement with ammonia at the 6-position before selective oxidation with bromine at the 8-position gave **5** in 59% yield over two steps as single regioisomer. A second S_NAr displacement with 4-chlorobenzylamine gave the key covalent precursor **6** in 66% yield. To synthesize the lysine-targeting warhead, the nitrile moiety of **6** was hydrolyzed under basic conditions to give benzoic acid **7**, which then underwent coupling with 4-fluorophenol using standard HATU conditions, and following acetonide deprotection, gave the second-generation TCI **8** in seven steps and 5% overall yield. Deprotection of the intermediate **6** gave the reversible molecular matched pair (MMP) **9** in 47% yield.

Characterization of the Second-Generation TCI 8. To investigate the reversible affinity and the potential to form a covalent bond with Lys56 in HSP72-NBD with our second-generation TCI **8** (Table 1, entry 3; Table 2, entry 2), we repeated our previously described analysis using the nucleotide-derived FP-assay, comparing the data to the first-generation TCI **2** (Table 1, entry 1; Table 2, entry 1). Briefly, displacement of the nucleotide-derived FP probe by the ligand was used to determine an apparent (App.) K_i.[27] Because the bound fraction of the probe is dependent on the effective concentration of the protein, a time-dependent decrease following covalent bond formation should result in a shift in the binding curve for the TCI. The time-dependent FP-assay data revealed that the initial reversible binding affinity of activated ester **8** displayed a 7-fold improvement over our first-generation TCI **2** but was >13-fold weaker than the tight-binding reversible nitrile MMP **9** (Table 1, entry 2; $pK_i > 6.70$, $K_i = <0.20\ \mu M$, $N = 3$). Disappointingly, there was no clear time dependence in the App. K_i, and consistent with this result, analysis of the intact-protein MS data for **8** also revealed no evidence of specific and selective covalent-bond formation.

From these data, we concluded that although our TCI design was successful in predicting that the binding site could accommodate the activated ester and maintain reversible

DOI: 10.1021/acs.jmedchem.9b01709
J. Med. Chem. 2019, 62, 11383−11398

affinity, we had failed to account for the stereoelectronic requirements of the electrophile. Efficient nucleophilic addition to the carbonyl must satisfy the correct Bürgi−Dunitz[33] and Flippin−Lodge angles[34] at appropriate reaction distances. This could not be achieved with *p*-fluorophenolate leaving group adopting the necessary vector-to-solvent in the conformationally restrictive TCI reversible binding mode, thus blocking covalent-bond formation and the E-I complex.

Design and Synthesis of the Third-Generation HSP72 TCI. The aryl sulfonyl fluoride electrophile has recently become popular in both synthetic chemistry and chemical biology.[35,36] Sulfonyl fluorides are stable in water under physiologically relevant conditions and have previously been shown to react readily with lysine residues in proteins.[35,36] A recent study by Grimster et al. demonstrated that the electrophilicity of the moiety displays a strong dependence on the electronics of the attached aromatic ring and can be modulated to give an intrinsic reactivity against glutathione, comparable to chemical probe-relevant *N*-arylacrylamide electrophiles.[37] The solvation-dependent fluoride leaving group is less likely to form a steric clash, and the proposed S_AN associative mechanism[38] should allow for a less restrictive stereoelectronic requirement for the reaction in the conformationally rigid protein-binding site. We therefore hypothesized that incorporation of an aryl sulfonyl fluoride electrophile would be effective in our Lys56-targeting HSP72 third-generation TCI. Unfortunately, our current methodology for the synthesis of 5′-benzylriboside ethers proved incompatible with the incorporation of the sulfonyl fluoride electrophile, so we adapted our TCI design to include an ester linker.

2′,3′-Acetonide-protected adenosine **10** was selectively oxidized with bromine to give **11** in moderate yield. S_NAr displacement with 4-chlorobenzylamine gave **12**, which then underwent selective esterification with 4-(fluorosulfonyl)-benzoyl chloride to give **13** in 56% yield. The sulfonyl fluoride electrophile proved stable to the acetonide-deprotection conditions and gave the third-generation TCI **14**, following treatment with TFA/H_2O, in four steps and 13% overall yield. To determine the effect of the 5′-ester linker on the reversible affinity, we synthesized the noncovalent ester MMP **15** of ether **9** in two steps from the primary alcohol intermediate **12** in 16% yield using 4-cyanobenzoyl chloride (Scheme 2).

Characterization of the Third-Generation TCI. The reversible 5′-ester analogue **15** displayed a binding affinity of K_i = 3.5 μM (pK_i = 5.45 ± 0.01, N = 3), >18-fold less potent than the tight-binding ether MMP **9** but sufficiently potent to investigate the role of the electrophile in HSP72 TCI design. Therefore, the third-generation ester sulfonyl fluoride TCI **14** was analyzed in the HSP72-NBD FP-assay. Pleasingly, **14** displayed a clear time-dependent shift in the probe displacement curve, consistent with covalent bond formation. The App. K_i = 17 μM observed after 5 min exposure of TCI **14** was comparable to the reversible ester analogue **15**. The App. K_i appeared to increase in activity 24-fold over 2 h. The MMP irreversible control **13** showed no reversible binding affinity and no time-dependent displacement of the FP-probe. The analysis was repeated using the HSP72-NBD K56A mutant (see the Supporting Information):[20] no time-dependent shift in the probe displacement curve was observed, suggesting no significant formation of the covalent adduct with TCI **14** under the same conditions as the WT-HSP72-NBD, confirming the reaction specificity and requirement for an initial reversible binding event.

To confirm these results were due to covalent-bond formation, we then analyzed the reaction by intact-protein MS. A solution of HSP72-NBD and *p*-sulfonyl fluoride (SF) TCI **14** (20 μM **14** and 2.0 μM HSP72-NBD) was incubated at 21 °C (room temperature) for 2 h. The experiment was repeated with irreversible control **13** under the same conditions. These data revealed that SF TCI **14** formed a covalent bond with HSP72-NBD, with the reaction going apparently to completion within 3 h of exposure using this semiquantitative assessment. The irreversible control MMP **13** gave no reaction under these conditions.

Covalent FP-Assay. The timeframe of the App. K_i shift and intact-protein MS with the third-generation SF TCI **14** strongly indicated that it was far more efficient than the first-generation acrylate TCI **2** (Table 2, entry 1 vs Table 2, entry 4), as the formation of the covalent adduct was reduced from days to hours. However, using these data alone, it was not possible to quantify this optimization or to determine whether the increased activity was due to an increase in the reversible binding affinity K_I, an increase in efficiency of the covalent reaction k_{inact}, or a mixture of the two, although analysis of the early time point App. K_i values did suggest the two analogues might possess comparable reversible affinity. To deconvolute the TCI optimization, it would be necessary to develop a new method to determine the kinetic parameters involved in the irreversible inhibition of HSP72-NBD.

Determining the kinetic parameters involved in covalent bond formation with proteins can be challenging.[39] Kinetic data often relies upon reaction rate changes evaluated from secondary readouts, such as substrate to product formation. While this analysis can be accurate in determining the key second-order rate constant for the process, k_{inact}/K_I, it can be difficult to accurately distinguish whether the retardation of the substrate to product reaction rate is due to reversible target occupancy or irreversible covalent bond formation. When attempting to determine k_{inact}, the reversible target occupancy is very high and approaches saturation, which significantly slows the substrate to product reaction separately from the covalent occupancy. Under these conditions, the time-dependent change in the rate of substrate to product reaction, necessary to determine k_{inact}, is unavoidably very small and difficult to quantify accurately.[9] This can lead to a significant underestimation of k_{inact} and a resulting overestimation of the binding affinity, K_I. While a direct measurement of the rate of protein−TCI covalent adduct formation, the actual product of interest, using quantified mass spectrometry would circumvent many of these challenges, though determining kinetic parameters for tight-binding and high-k_{inact} TCIs would still be difficult, this method is typically low-throughput and cannot observe noncovalent adducts due to the denaturing conditions of the assay. Therefore, TCI reversible affinities cannot be simply compared to their reversible noncovalent MMPs, a crucial requirement for efficient optimization.

Following analysis of the nucleotide-derived HSP72-NBD FP-assay, we hypothesized that it could be adapted to determine the kinetic parameters of covalent bond formation and would allow us to directly compare TCIs with reversible analogues. The probe bound fraction (F_b) is determined by the affinity of the probe and the apparent concentration of the protein (see the Supporting Information for details).[27] Changes in the bound fraction of the probe are observed through changes in the polarization of light emitted. Crucially, changes in the bound fraction are proportional to the effective

DOI: 10.1021/acs.jmedchem.9b01709
J. Med. Chem. 2019, 62, 11383−11398

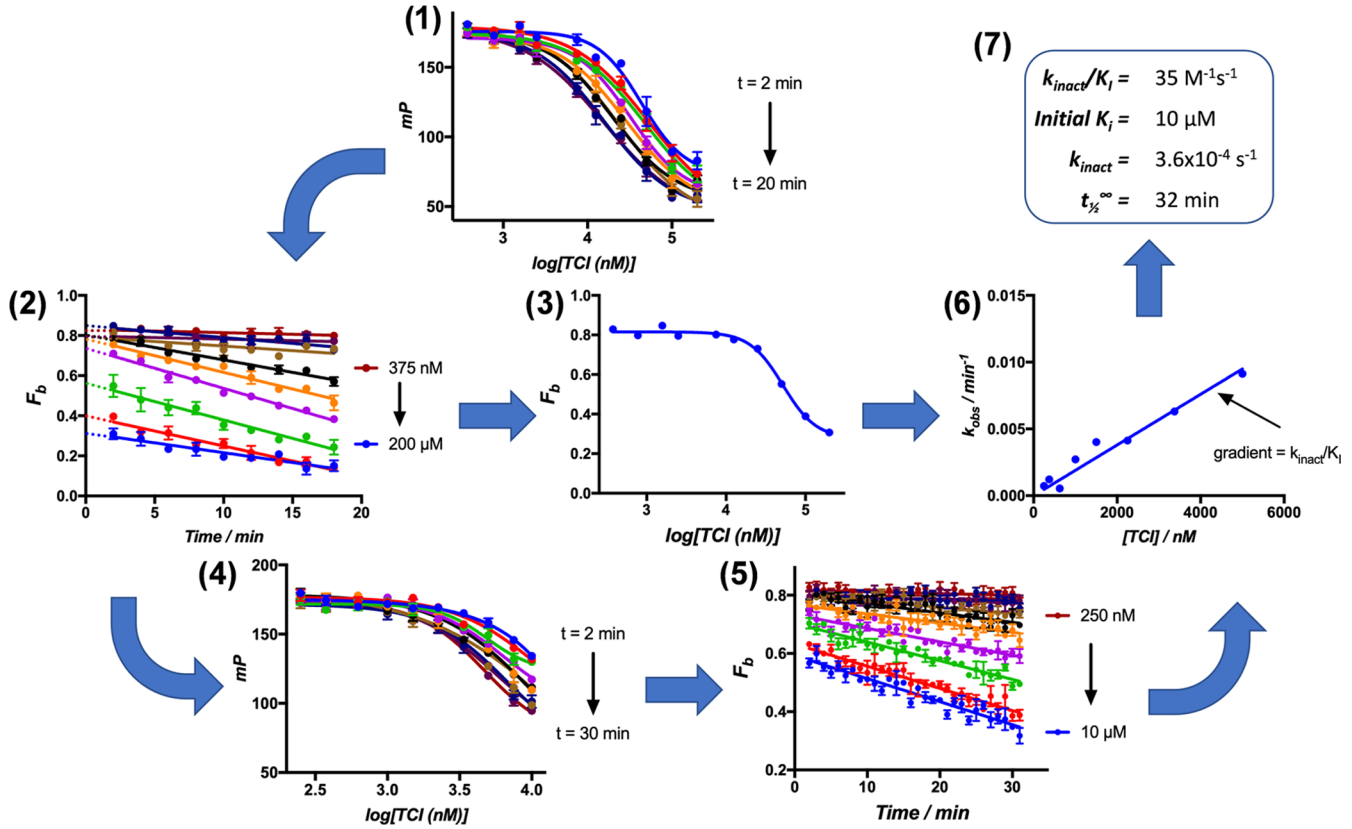

Figure 4. Covalent FP-assay to determine the efficiency of covalent-bond formation. (1) Initial titration across a wide range of TCI concentrations and timepoints. (2) Extrapolation of the time-dependent change in F_b to t = 0. (3) Estimation of initial K_i from extrapolated $t = 0$ F_b values; for an example of how to determine K_i from an IC_{50} in the FP-assay, see the Supporting Information.[27] (4) Second focused titration on concentrations of TCI < K_i. (5) Gradient of time-dependent change in F_b used to calculate k_{obs} at a given concentration of TCI. (6) The gradient of the rate of change of k_{obs} with [TCI] determines the second-order rate constant k_{inact}/K_I. (7) By assuming $K_i = K_I$, k_{inact} can be calculated from k_{inact}/K_I and converted to $t_{1/2}^{inf}$. See the Supporting Information for details.

concentration of protein. Displacement of the FP-probe by an inhibitor essentially decreases the effective concentration of protein, resulting in a decrease in the bound fraction. For a reversible inhibitor at equilibrium, the bound fraction remains constant at a given concentration. For an irreversible covalent inhibitor, the effective protein concentration decreases with time, which must result in a decrease in bound fraction. The time-dependent change in probe bound fraction could therefore be used to quantify the covalent-bond formation without secondary product formation or MS analysis.

To quantify the covalent bond formation for our TCIs with HSP72-NBD, we would need to interpret the time-dependent change in polarization of light from the probe. The polarization must first be converted into the anisotropy, as the bound fraction of the fluorescent probe is directly proportional to the anisotropy (A). However, F_b displays a nonlinear relationship with the effective protein concentration (E) such that at high bound fractions ($F_b > 0.8$), small changes in anisotropy would equate to very large changes in effective protein concentration, resulting in low accuracy. At low bound fractions ($F_b < 0.4$), large changes in anisotropy would be needed to observe a small change in effective protein concentration, which would result in low sensitivity (see the Supporting Information). Between these two extremes, the response of bound fraction to changes in the effective protein concentration are linear to an acceptable approximation.[27]

To develop the HSP72 covalent FP-assay, we selected an initial protein concentration that would lead to a high bound fraction ($F_b = 0.8$), as the reversible occupancy of the protein would rapidly displace the probe and reduce F_b. If the initial effective protein concentration was too low, this reversible displacement would move our analysis outside of the linear quantification window of the assay. As the concentration of the TCI is increased, the rate of change of F_b will increase. Following extrapolation of the linear regression to $t = 0$, the initial F_b values are then plotted against the TCI concentration to generate a displacement curve and calculate the initial K_i. This quantifies the reversible affinity of the ligand, prior to the formation of the covalent bond and depletion of the effective protein concentration. The initial K_i value is then used to focus a second FP titration at TCI concentrations below initial K_i to estimate the crucial second-order rate constant k_{inact}/K_I. Linear regression on the F_b versus time graph will give the rate of change of F_b, which is converted into the pseudo-first-order rate constant k_{obs}, using the F_b values extrapolated from $t = 0$. Finally, the plot of k_{obs} against the TCI concentration would give k_{inact}/K_I from the gradient of the linear region of the graph, and by assuming $K_I = K_i$, we can estimate k_{inact} from this relationship and the initial K_i (Figure 4).

Kinetic Characterization of the Lysine-Targeting TCIs. Using our analysis from the covalent FP-assay, third-generation aryl-SF TCI **14** displayed a second-order rate constant for the efficiency of the covalent-bond formation with HSP72-NBD[40] of $k_{inact}/K_I = 35 \pm 1.7$ M^{-1} s^{-1} and k_{inact} calculated as 3.6×10^{-4} s^{-1}, equivalent to $t_{1/2}^{inf} = 32$ min (Table 1, entry 6). The half-life from the covalent FP-assay was consistent with the data

DOI: 10.1021/acs.jmedchem.9b01709
J. Med. Chem. 2019, 62, 11383−11398

from our intact-protein MS assay (Table 2, entry 4) that showed complete modification of HSP72-NBD by SF TCI **14** (20 μM, 2 × initial K_i) within 3 h (5.6 half-lives).

Comparing to the first-generation acrylate TCI **2** (Table 1, entry 1; Table 2, entry 1): the aryl-SF-TCI **14** displayed a 41-fold increase in k_{inact}/K_I, consistent with the time-dependent shift observed in the FP-assay. However, this improvement in covalent efficiency was not due to an increase in reversible affinity, as initial K_i only increased by 1.8-fold. The optimization of k_{inact}/K_I was derived largely by an improved k_{inact} (23-fold increase). The negative-control MMP of aryl-SF **14**, acetonide **13**, displayed no reactivity with accessible nucleophilic residues on HSP72-NBD to form a covalent adduct when assessed by intact protein MS, which suggested that the compatibility of the harder lysine electrophile was the driver of k_{inact} rather than intrinsic reactivity.

***K*$_I$ Optimization of the Third-Generation Aryl-SF TCI.** Exploiting the versatility of the covalent FP-assay to directly compare covalent and noncovalent ligands, we designed a series of 5′-aryl-SF TCI analogues based on the known affinities of their reversible MMPs. Substitution at the 8-position of the adenine ring is essential for the affinity of this class of inhibitors, and these diverse structures are synthetically tractable (Scheme 2).[18,23,41,42]

Analysis of the kinetics of the Lys56-targeting HSP72-NBD TCI series revealed that k_{inact} was comparable across the three aryl-SF analogues where a value could be determined (Table 1, entries 6 and 8−9). The 8-nonsubstituted analogue **16** displayed an activity 70-fold weaker than that of *N*-4-chlorobenzyl TCI **14**, demonstrating the importance of reversible affinity for TCI efficiency against this target. The 8-*N*-methyl-substituted analogue **17** decreased the covalent efficiency of the TCI 11-fold, which was predominately due to a drop in initial K_i consistent with the reported activity of its reversible MMP.[23] Finally, substitution with the 8-*N*-quinoline moiety, an analogue previously demonstrated to display the highest affinity as a reversible MMP,[41] to give **18**, enhanced k_{inact}/K_I 2.7-fold compared to the *p*-chloro aryl-SF TCI **14**, consistent with the 2.1-fold improvement in reversible affinity, and representing a 108-fold enhancement in covalent efficiency over our first-generation acrylate TCI **2**.

CONCLUSIONS

The design, application, and analysis of TCIs in a rational and quantitative manner remain a critical challenge in covalent inhibitor drug discovery. The covalent FP-assay we developed utilized the time-dependent change in FP-probe bound fraction to determine the fundamental parameters of covalent-bond formation. For proteins like HSP72 with poor catalytic turnover in biochemical assays or nonenzymatic receptors and scaffolding proteins, the covalent FP-assay will be an important addition to the available methods to quantify and deconvolute the activity of TCIs, particularly as noncovalent reversible MMPs can be directly compared without the need to change assay formats.

We exploited our novel covalent FP-assay to continue our development of methods and strategies to discover lysine-targeting covalent inhibitors. Through our exhaustive understanding of the SAR and binding mode of nucleoside-derived reversible ligands of HSP72, we designed a next-generation sulfonyl fluoride TCI **18**, which displayed a 108-fold enhancement in the critical second-order rate constant, k_{inact}/K_I. Further analysis revealed that the rate enhancement was due to both optimization of K_I, in a manner consistent with their MMP reversible analogues, and through a significant increase in k_{inact}. The failure of our activated ester second-generation TCI **8** demonstrates the importance of electrophile design when targeting the harder nucleophile in lysine residues. The angles of attack in a conformationally restrictive environment, while maintaining the vectors and steric requirements to accommodate a leaving group, makes the design of lysine-selective electrophiles challenging. The sulfonyl fluoride electrophile was able to circumvent many of these difficulties, with its small fluoride leaving group and accommodating sulfur electrophilic center, and this represents a key learning in lysine electrophile design. As we continue to progress toward a cell active chemical probe for HSP72 and as we improve our understanding and design strategy toward lysine-targeting covalent inhibitors of other challenging targets, the nature of the electrophile will prove crucial if we are to be successful.

EXPERIMENTAL SECTION

General Experimental. Unless otherwise stated, reactions were conducted in oven-dried glassware under an atmosphere of nitrogen or argon using anhydrous solvents. All commercially obtained reagents and solvents were used as received. Thin-layer chromatography (TLC) was performed on precoated aluminum sheets of silica (60 F254 nm, Merck) and visualized using short-wave UV light. Flash column chromatography was carried out on Merck silica gel 60 (partial size, 40−65 μm). Column chromatography was also performed on a Biotage SP1 or Biotage Isolera Four purification system using Biotage Flash silica cartridges (SNAP KP-Sil) or for reverse-phase purifications SNAP Ultra C18 cartridges. Ion-exchange chromatography was performed using acidic Isolute Flash SCX-II columns. ^{1}H NMR spectra were recorded on Bruker AMX500 (500 MHz) spectrometers using an internal deuterium lock. Chemical shifts are quoted in parts per million (ppm) using the following internal references: $CDCl_3$ (δH 7.26), MeOD (δH 3.31), and dimethyl sulfoxide (DMSO)-d_6 (δH 2.50). Signal multiplicities are recorded as singlet (s), doublet (d), triplet (t), quartet (q), multiplet (m), doublet of doublets (dd), doublet of doublet of doublets (ddd), broad (br), apparent (app), or obscured (obs). Coupling constants, J, are measured to the nearest 0.1 Hz. ^{13}C NMR spectra were recorded on Bruker AMX500 spectrometers at 126 MHz using an internal deuterium lock. Chemical shifts are quoted to 0.01 ppm, unless greater accuracy was required, using the following internal references: $CDCl_3$ (δC 77.0), MeOD (δC 49.0), and DMSO-d_6 (δC 39.5). High-resolution mass spectra were recorded on an Agilent 1200 series HPLC and diode array detector coupled to a 6210 time-of-flight mass spectrometer with dual multimode APCI/ESI source or on a Waters Acquity UPLC and diode array detector coupled to a Waters G2 QToF mass spectrometer fitted with a multimode ESI/APCI source. For HRMS and liquid chromatography-mass spectrometry (LCMS) extended mass (100−1000 AMU), analytical separation was carried out at 30 °C on a Merck Chromolith Flash column (RP-18e, 25 mm × 2 mm) using a flow rate of 0.75 mL/min in a 4 min gradient elution with detection at 254 nm. The mobile phase was a mixture of methanol (solvent A) and water (solvent B), both containing formic acid at 0.1%. Gradient elution was as follows: 5:95 (A/B) to 100:0 (A/B) over 2.5 min, 100:0 (A/B) for 1 min, and then reversion back to 5:95 (A/B) over 0.1 min, finally 5:95 (A/B) for 0.4 min. HRMS references: caffeine $[M + H]^+$ 195.087652; hexakis (2,2-difluroethoxy)phosphazene $[M + H]^+$ 622.02896; and hexakis(1*H*,1*H*,3*H*-tetrafluoropentoxy)phosphazene $[M + H]^+$ 922.009798. For standard LCMS, analytical separation was carried out at 40 °C on a Merck Chromolith Flash column (RP-18e, 25 mm × 2 mm) using a flow rate of 1.5 mL/min in a 2 min gradient elution with detection at 254 nm. The mobile phase was a mixture of methanol (solvent A) and water (solvent B), both containing formic acid at 0.1%. Gradient elution was as follows: 5:95 (A/B) to 100:0 (A/B) over 1.25 min, 100:0 (A/B) for 0.5 min, and then reversion back to 5:95 (A/B) over 0.05 min, finally 5:95 (A/B) for 0.2 min. Infrared spectra were

DOI: 10.1021/acs.jmedchem.9b01709
J. Med. Chem. 2019, 62, 11383−11398

recorded on a Bruker α-p Fourier transform infrared (FT-IR) spectrometer. Absorption maxima (ν_{max}) are quoted in wavenumbers (cm^{-1}). All compounds were found to be >95% pure by HPLC analysis unless otherwise stated. The standard adenine and adenosine numbering has been used throughout. All compounds were found to be >95% pure by LCMS analysis unless otherwise stated.

4-((((2R,3S,4R,5R)-5-(6-amino-8-((3,4-dichlorobenzyl)amino)-9H-purin-9-yl)-3,4-dihydroxytetrahydrofuran-2-yl)methoxy)methyl)-benzonitrile ***1***. Synthesized via the method described by Williamson et al.[18]

3-((2R,3S,4R,5R)-5-(6-amino-8-((4-chlorobenzyl)amino)-9H-purin-9-yl)-3,4-dihydroxytetrahydrofuran-2-yl)propyl acrylate ***2***. Synthesized via the method described by Pettinger et al.[20]

4-((((3aR,4R,6R,6aR)-6-(6-chloro-9H-purin-9-yl)-2,2-dimethyltetrahydrofuro[3,4-d][1,3]dioxol-4-yl)methoxy)methyl)-benzonitrile ***4***. 6-Chloro-9-[2,3-*O*-(1-methylethylidene)-β-D-ribofuranosyl]-9*H*-Purine **3** (3.05 g, 9.34 mmol) and 4-(bromomethyl)-benzonitrile (7.33 g, 37.4 mmol) were dissolved in DMF (80 mL) and stirred at room temperature for 5 min. Sodium hydride (60% in mineral oil, 0.41 g, 10.3 mmol) was then added, and the reaction was stirred at room temperature for a further 45 min. The reaction was quenched with 1% AcOH (20 mL), then taken up in EtOAc (60 mL) and water (60 mL). The organic extracts were washed with sat. NaCl (3 × 50 mL) and dried over $MgSO_4$. The solvent was then removed under reduced pressure to give the crude product, which was purified by silica gel chromatography with the Biotage SP1 purification system (Cyc/EtOAc 100:0 to 70:30) to give the title compound **4** as a colorless foam (2.3 g, 56%); ^{1}H NMR (600 MHz, $CDCl_3$) δH 8.73 (s, 1H), 8.30 (s, 1H), 7.55 (d, *J* = 8.3 Hz, 2H), 7.23 (d, *J* = 8.2 Hz, 2H), 6.23 (d, *J* = 2.3 Hz, 1H), 5.38 (dd, *J* = 6.1, 2.3 Hz, 1H), 5.00 (dd, *J* = 6.1, 2.5 Hz, 1H), 4.59 (app. dt, *J* = 4.1, 2.9 Hz, 1H), 4.50 (d, *J* = 12.7 Hz, 1H), 4.47 (d, *J* = 12.7 Hz, 1H), 3.75 (dd, *J* = 10.5, 3.1 Hz, 1H), 3.68 (dd, *J* = 10.6, 4.2 Hz, 1H), 1.64 (s, 3H), 1.42 (s, 3H); ^{13}C NMR (151 MHz, CDCl3) δC 152.21, 151.36, 151.05, 143.87, 142.34, 132.39, 127.82, 118.83, 118.61, 114.68, 112.02, 92.38, 86.40, 84.92, 81.79, 72.78, 71.01, 27.29, 25.50; HRMS (ESI) $C_{21}H_{21}N_5O_4{}^{35}Cl$ ($M + H^+$) requires 442.1277, found 442.1254; t_R (LCMS) = 1.39 min.

4-((((3aR,4R,6R,6aR)-6-(6-amino-8-bromo-9H-purin-9-yl)-2,2-dimethyltetrahydrofuro[3,4-d][1,3]dioxol-4-yl)methoxy)methyl)-benzonitrile ***5***. 4-((((3*aR*,4*R*,6*R*,6*aR*)-6-(6-chloro-9*H*-purin-9-yl)-2,2-dimethyltetrahydrofuro[3,4-*d*][1,3]dioxol-4-yl)methoxy)methyl)-benzonitrile **4** (2.3 g, 5.21 mmol) was dissolved in ammonia (7 N in MeOH, 20 mL, 140 mmol) and heated in microwave at 110 °C for 2 h. The solvent was removed under reduced pressure, and the subsequent residue was partitioned between EtOAc (50 mL) and water (50 mL). The combined organic extracts were washed with sat. NaCl (3 × 30 mL) and dried over $MgSO_4$. The solvent was then removed under reduced pressure to give the crude product, which was purified by silica gel chromatography with the Biotage SP1 purification system (EtOAc/EtOH 100:0 to 60:40) to give 4-((((3*aR*,4*R*,6*R*,6*aR*)-6-(6-amino-9*H*-purin-9-yl)-2,2-dimethyltetrahydrofuro[3,4-*d*][1,3]dioxol-4-yl)-methoxy)methyl)benzonitrile as a white amorphous solid (1.81 g, 82%); ^{1}H NMR (600 MHz, $CDCl_3$) δH 8.30 (s, 1H), 7.92 (s, 1H), 7.54 (d, *J* = 8.3 Hz, 2H), 7.26 (obs. d, *J* = 8.0 Hz, 2H), 6.13 (d, *J* = 2.1 Hz, 1H), 5.58 (br. s, 2H), 5.44 (dd, *J* = 6.2, 2.2 Hz, 1H), 5.04 (dd, *J* = 6.2, 3.0 Hz, 1H), 4.55−4.48 (m, 3H), 3.73 (dd, *J* = 10.4, 3.8 Hz, 1H), 3.67 (dd, *J* = 10.4, 5.5 Hz, 1H), 1.63 (s, 3H), 1.41 (s, 3H); ^{13}C NMR (151 MHz, $CDCl_3$) δC 155.45, 153.25, 149.46, 142.99, 139.74, 132.30, 127.74, 120.33, 118.85, 114.50, 111.69, 91.56, 86.36, 84.60, 81.91, 72.60, 70.96, 27.32, 25.56; HRMS (ESI) $C_{21}H_{23}N_6O_4$ ($M + H^+$) requires 423.1775, found 423.1745; t_R (LCMS) = 1.24 min; IR (FTIR-ATR)/cm^{-1} = 3313, 3141, 2987, 2938, 2230, 1641, 1600, 1470, 1417, 1373. 4-((((3*aR*,4*R*,6*R*,6*aR*)-6-(6-amino-9*H*-purin-9-yl)-2,2-dimethyltetrahydrofuro[3,4-*d*][1,3]dioxol-4-yl)methoxy)methyl)-benzonitrile (1.62 g, 3.84 mmol) was dissolved in 1,4-dioxane (35.0 mL). To a solution of $K_2HPO_4{\cdot}3H_2O$ (2.63 g, 11.53 mmol) and bromine (1.54 g, 9.60 mmol) in water (35.0 mL) was then added dropwise to the stirred solution of 100 at room temperature. After 1 h, the reaction was quenched with sat. aq. $Na_2S_2O_3$ solution (40 mL) and stirred for a further 2 min. The resulting mixture was extracted with EtOAc (3 × 50 mL), then the combined organic layers were washed with sat. NaCl (3 × 50 mL) and dried over $MgSO_4$. The solvent was then removed under reduced pressure to give the crude product, which was purified by silica gel chromatography with the Biotage SP1 purification system (Cyc/EtOAc 50:50 to 0:100) to give the title compound **5** as a yellow oil (1.39 g, 72%); ^{1}H NMR (600 MHz, $CDCl_3$) δH 8.16 (s, 1H), 7.54 (d, *J* = 8.3 Hz, 2H), 7.30 (d, *J* = 8.4 Hz, 2H), 6.21 (d, *J* = 1.7 Hz, 1H), 5.67 (dd, *J* = 6.4, 1.8 Hz, 1H), 5.61 (br. s, 2H), 5.16 (dd, *J* = 6.3, 3.8 Hz, 1H), 4.54 (d, *J* = 13.3 Hz, 1H), 4.48 (d, *J* = 13.3 Hz, 1H), 4.44 (app. dt, *J* = 7.5, 4.5 Hz, 1H), 3.67 (dd, *J* = 10.3, 4.8 Hz, 1H), 3.60 (dd, *J* = 10.3, 7.4 Hz, 1H), 1.63 (s, 3H), 1.40 (s, 3H); ^{13}C NMR (151 MHz, $CDCl_3$) δC 154.24, 152.97, 150.51, 143.49, 132.22, 127.88, 127.73, 120.30, 118.96, 114.57, 111.47, 91.37, 86.98, 83.47, 82.21, 72.37, 70.64, 27.34, 25.60; HRMS (ESI) $C_{21}H_{22}N_6O_4{}^{79}Br$ ($M + H^+$) requires 501.0880, found 501.0871; t_R (LCMS) = 1.46 min; IR (FTIR-ATR)/cm^{-1} = 3322, 3172, 2987, 2228, 1639, 1597, 1577, 1454, 1373, 1290, 1205.

4-((((3aR,4R,6R,6aR)-6-(6-amino-8-((4-chlorobenzyl)amino)-9H-purin-9-yl)-2,2-dimethyltetrahydrofuro[3,4-d][1,3]dioxol-4-yl)-methoxy)methyl)benzonitrile ***6***. 4-((((3*aR*,4*R*,6*R*,6*aR*)-6-(6-amino-8-bromo-9*H*-purin-9-yl)-2,2-dimethyltetrahydrofuro[3,4-*d*][1,3]-dioxol-4-yl)methoxy)methyl)benzonitrile **5** (0.98 g, 1.95 mmol) was dissolved in EtOH (16 mL) and added to 4-chlorobenzylamine (2.77 g, 19.5 mmol), and the reaction was heated in microwave for 1 h at 160 °C. The solvent was removed under reduced pressure, and the resulting residue was taken up in EtOAc (50 mL) and 1% aq. AcOH (50 mL). The product was extracted with EtOAc (3 × 40 mL); washed with 1% aq. AcOH (3 × 40 mL), sat. $NaHCO_3$ (3 × 40 mL) and sat. NaCl (40 mL); and dried over Na_2SO_4. The solvent was removed under reduced pressure, and the crude product was purified by silica gel chromatography with the Biotage SP1 purification system (EtOAc/EtOH 100:0 to 80:20) to give the title compound **6** as an orange foam (0.72 g, 66%); ^{1}H NMR (600 MHz, $CDCl_3$) δH 8.17 (s, 1H), 7.55 (d, *J* = 8.3 Hz, 2H), 7.25 (d, *J* = 8.4 Hz, 2H), 7.19−7.15 (m, 4H), 6.23 (d, *J* = 3.3 Hz, 1H), 5.90 (app. t, *J* = 5.9 Hz, 1H), 5.33 (dd, *J* = 6.7, 3.3 Hz, 1H), 5.15 (br. s, 2H), 4.97 (dd, *J* = 6.7, 3.9 Hz, 1H), 4.45 (dd, *J* = 15.6, 6.0 Hz, 1H), 4.42 (dd, *J* = 15.5, 5.6 Hz, 1H), 4.30−4.26 (m, 3H), 3.73 (dd, *J* = 10.5, 3.0 Hz, 1H), 3.57 (dd, *J* = 10.5, 2.9 Hz, 1H), 1.62 (s, 3H), 1.38 (s, 3H); ^{13}C NMR (151 MHz, $CDCl_3$) δC 152.18, 151.61, 150.34, 150.28, 142.30, 137.35, 133.37, 132.52, 128.87, 128.69, 127.74, 118.60, 117.58, 115.34, 112.08, 88.63, 83.86, 82.82, 80.14, 72.60, 69.50, 46.06, 27.41, 25.58; HRMS (ESI) $C_{28}H_{29}N_7O_4{}^{35}Cl$ ($M + H^+$) requires 562.1964, found 562.1922; t_R (LCMS) = 1.48 min; IR (FTIR-ATR)/cm^{-1} = 3325, 2934, 2229, 1633, 1606, 1571, 1491, 1469, 1434, 1361, 1333, 1285, 1210.

4-((((3aR,4R,6R,6aR)-6-(6-amino-8-((4-chlorobenzyl)amino)-9H-purin-9-yl)-2,2-dimethyltetrahydrofuro[3,4-d][1,3]dioxol-4-yl)-methoxy)methyl)benzoic acid ***7***. 4-((((3*aR*,4*R*,6*R*,6*aR*)-6-(6-amino-8-((4-chlorobenzyl)amino)-9*H*-purin-9-yl)-2,2-dimethyltetrahydrofuro[3,4-*d*][1,3]dioxol-4-yl)methoxy)methyl)-benzonitrile **6** (91 mg, 0.16 mmol) was dissolved in aq. NaOH (2 M, 0.8 mL, 1.62 mmol) and ethanol (0.9 mL) and heated in a sealed microwave vial at 110 °C for 3 h. The reaction was cooled to room temperature and neutralized to pH 7 with 1 M HCl. The mixture was extracted with EtOAc (3 × 20 mL), and the combined organic extracts were washed with sat. aq. $NaHCO_3$ (3 × 20 mL) and sat. NaCl (3 × 20 mL) and dried over $MgSO_4$. The solvent was then removed under reduced pressure to give the crude product, which was purified by reverse-phase C18 chromatography with the Biotage SP1 purification system (water/MeCN 70:30 to 0:100) to give the title compound **7** as a white amorphous solid (55 mg, 58%); ^{1}H NMR (600 MHz, $CDCl_3$) δH 8.03 (s, 1H), 7.94 (d, *J* = 8.2 Hz, 2H), 7.24 (d, *J* = 8.4 Hz, 2H), 7.13 (d, *J* = 8.2 Hz, 2H), 7.10 (d, *J* = 7.9 Hz, 2H), 6.49 (br. s, 2H), 6.16 (d, *J* = 2.8 Hz, 1H), 6.05 (app. t, *J* = 6.0 Hz, 1H), 5.59 (dd, *J* = 6.4, 2.9 Hz, 1H), 5.01 (dd, *J* = 6.5, 3.2 Hz, 1H), 4.42−4.24 (m, 5H), 3.73 (dd, *J* = 10.6, 2.8 Hz, 1H), 3.64 (dd, *J* = 10.5, 3.0 Hz, 1H), 1.62 (s, 3H), 1.40 (s, 3H); ^{13}C NMR (151 MHz, $CDCl_3$) δC 170.16, 152.14, 151.89, 149.52, 148.83, 141.29, 137.12, 133.33, 131.51, 130.14, 128.83, 128.71, 127.41, 116.69, 114.82, 89.87, 84.99, 82.80, 80.67, 73.51, 69.79, 45.80, 27.33, 25.55; t_R (LCMS) = 1.47 min.

DOI: 10.1021/acs.jmedchem.9b01709
J. Med. Chem. 2019, 62, 11383−11398

4-fluorophenyl 4-((((2R,3S,4R,5R)-5-(6-amino-8-((4-chlorobenzyl)amino)-9H-purin-9-yl)-3,4-dihydroxytetrahydrofuran-2-yl)methoxy)methyl)benzoate **8**. 4-((((3*aR*,4*R*,6*R*,6*aR*)-6-(6-amino-8-((4-chlorobenzyl)amino)-9*H*-purin-9-yl)-2,2-dimethyltetrahydrofuro[3,4-*d*][1,3]dioxol-4-yl)methoxy)methyl)-benzoic acid **7** (20 mg, 34 μmol) was dissolved in DMF (0.4 mL). HATU (16 mg, 41 μmol) and DIPEA (9 mg, 69 μmol) were added, and the reaction was stirred at room temperature for 1 min. 4-Fluorophenol (12 mg, 0.10 mmol) was added, and the reaction was stirred at room temperature for 18 h. The solvent was then removed under reduced pressure to give the crude product, which was purified by silica gel chromatography with the Biotage SP1 purification system (EtOAc/EtOH 100:0 to 80:20) to give 4-fluorophenyl 4-((((3*aR*,4*R*,6*R*,6*aR*)-6-(6-amino-8-((4-chlorobenzyl)amino)-9*H*-purin-9-yl)-2,2-dimethyltetrahydrofuro[3,4-*d*][1,3]dioxol-4-yl)-methoxy)methyl)benzoate as a yellow oil (11 mg, 47%); ^{1}H NMR (600 MHz, DMSO-d_6) δH 8.03 (d, *J* = 8.3 Hz, 2H), 7.89 (s, 1H), 7.49 (app. t, *J* = 6.0 Hz, 1H), 7.41 (d, *J* = 8.1 Hz, 2H), 7.40−7.28 (m, 8H), 6.52 (br. s, 2H), 6.13 (d, *J* = 2.4 Hz, 1H), 5.70 (dd, *J* = 6.3, 2.4 Hz, 1H), 5.07 (dd, *J* = 6.3, 3.3 Hz, 1H), 4.58−4.47 (m, 4H), 4.29 (app. td, *J* = 5.5, 3.3 Hz, 1H), 3.65 (dd, *J* = 10.5, 5.1 Hz, 1H), 3.53 (dd, *J* = 10.5, 6.2 Hz, 1H), 1.54 (s, 3H), 1.34 (s, 3H); ^{13}C NMR (151 MHz, DMSO-d_6) δC 164.41, 152.56, 151.11, 149.20, 148.92, 146.69, 144.46, 138.71, 131.28, 129.81, 129.10, 128.10, 127.77, 127.38, 123.77 (d, *J* = 8.8 Hz), 117.06, 116.23, 116.08, 113.25, 87.51, 84.55, 81.89, 81.42, 71.54, 69.94, 44.72, 27.06, 25.29; ^{19}F NMR (471 MHz, DMSO-d_6) δF −117.07; HRMS (ESI) $C_{34}H_{33}N_6O_6{}^{35}ClF$ (M + H$^+$) requires 675.2129, found 675.2037; t_R (LCMS_extended) = 3.23 min. 4-fluorophenyl 4-((((3*aR*,4*R*,6*R*,6*aR*)-6-(6-amino-8-((4-chlorobenzyl)-amino)-9*H*-purin-9-yl)-2,2-dimethyltetrahydrofuro[3,4-*d*][1,3]dioxol-4-yl)methoxy)methyl)benzoate (5 mg, 7 μmol) was dissolved in a 5:2 mixture of TFA/H_2O (0.7 mL) and stirred at room temperature for 30 min. The solvent was then removed under reduced pressure to give the crude product, which was purified by reverse-phase C18 chromatography with the Biotage SP1 purification system (water/MeCN 80:20 to 0:100) to give the title compound **8** as a white amorphous solid (4 mg, 85%); ^{1}H NMR (600 MHz, DMSO-d_6) δH 8.02 (d, *J* = 8.3 Hz, 2H), 7.90 (s, 1H), 7.43 (d, *J* = 8.1 Hz, 2H), 7.36−7.29 (m, 8H), 7.13 (app. t, *J* = 6.0 Hz, 1H), 6.46 (br. s, 2H), 5.88 (d, *J* = 5.8 Hz, 1H), 5.47 (br. app. s, 1H), 5.29 (br. app. s, 1H), 4.94−4.88 (m, 1H), 4.59−4.53 (m, 2H), 4.52−4.44 (m, 2H), 4.33−4.28 (m, 1H), 4.07−4.02 (m, 1H), 3.78 (dd, *J* = 10.7, 3.1 Hz, 1H), 3.65 (dd, *J* = 10.8, 4.5 Hz, 1H); ^{13}C NMR (151 MHz, DMSO-d_6) δC 164.35, 152.47, 151.27, 149.92, 148.92, 146.67, 144.36, 138.79, 131.20, 129.82, 128.83, 128.07, 127.81, 127.41, 123.75 (d, *J* = 8.7 Hz), 116.91, 116.23, 116.07, 86.92, 82.86, 71.69, 70.49, 70.39, 44.61, 40.06; HRMS (ESI) $C_{31}H_{29}N_6O_6{}^{35}ClF$ (M + H$^+$) requires 635.1816, found 635.1823; t_R (LCMS) = 1.64 min.

4-((((2R,3S,4R,5R)-5-(6-amino-8-((4-chlorobenzyl)amino)-9H-purin-9-yl)-3,4-dihydroxytetrahydrofuran-2-yl)methoxy)methyl)-benzonitrile **9**. 4-((((3*aR*,4*R*,6*R*,6*aR*)-6-(6-amino-8-((4-chlorobenzyl)amino)-9*H*-purin-9-yl)-2,2-dimethyltetrahydrofuro[3,4-*d*][1,3]dioxol-4-yl)methoxy)methyl)benzonitrile **6** (25 mg, 45 μmol) was dissolved in a 5:2 mixture of TFA/H_2O (1.4 mL) and stirred at room temperature for 30 min. The solvent was then removed under reduced pressure to give the crude product, which was purified by reverse-phase C18 chromatography with the Biotage SP1 purification system (water/MeCN + 0.1% formic acid, 70:30 to 0:100) to give the title compound **9** as a colorless oil (11 mg, 47%); ^{1}H NMR (600 MHz, DMSO-d_6) δH 7.89 (s, 1H), 7.72 (d, *J* = 7.8 Hz, 2H), 7.38 (d, *J* = 7.9 Hz, 2H), 7.32 (d, *J* = 8.3 Hz, 2H), 7.29 (d, *J* = 8.3 Hz, 2H), 7.11 (app. t, *J* = 6.1 Hz, 1H), 6.47 (br. s, 2H), 5.86 (d, *J* = 5.6 Hz, 1H), 5.38 (d, *J* = 5.8, 1H), 5.21 (d, *J* = 5.2 Hz, 1H), 4.93 (app. q, *J* = 5.6 Hz, 1H), 4.55−4.49 (m, 2H), 4.49−4.41 (m, 2H), 4.31 (app. q, *J* = 5.0 Hz, 1H), 4.03 (app. q, *J* = 4.0 Hz, 1H), 3.76 (dd, J = 10.9, 3.1 Hz, 1H), 3.64 (dd, *J* = 10.8, 4.5 Hz, 1H); ^{13}C NMR (151 MHz, DMSO-d_6) δC 152.48, 151.30, 149.88, 148.91, 143.79, 138.75, 132.13, 131.22, 128.84, 128.07, 127.70, 118.75, 116.92, 110.11, 86.95, 82.78, 71.43, 70.46, 70.39, 70.28, 44.60; HRMS (ESI) $C_{25}H_{25}N_7O_4{}^{35}Cl$ (M + H$^+$) requires 522.1651, found 522.1570; t_R (LCMS) = 1.32 min; IR (FTIR-ATR)/cm^{-1} = 3432, 3325, 3232, 2925, 2230, 1651, 1612, 1595, 1573, 1531, 1490, 1443, 1333, 1299.

((3aR,4R,6R,6aR)-6-(6-amino-8-bromo-9H-purin-9-yl)-2,2-dimethyltetrahydrofuro[3,4-d][1,3]dioxol-4-yl)methanol **11**. 2′,3′-*O*-isopropylideneadenosine **10** (1.17 g, 3.81 mmol) was dissolved in 1,4-dioxane (16 mL) and stirred to dissolution. $K_2HPO_4{\cdot}3H_2O$ (2.61 g, 11.4 mmol) was dissolved in water (16 mL) and then added to bromine (1.52 g, 9.52 mmol). The bromine solution was added dropwise to the stirred adenosine solution at room temperature. After 30 min, the reaction was quenched with sat. aq. $Na_2S_2O_3$ solution (30 mL) and stirred for a further 2 min. The resulting mixture was extracted with EtOAc (3 × 100 mL), then the combined organic layers washed with sat. NaCl and dried over Na_2SO_4. The solvent was removed under reduced pressure, and the crude product was purified by silica gel chromatography with the Biotage SP1 purification system (EtOAc/EtOH 100:0 to 80:20) to give the title compound **11** as an orange solid (1.1 g, 74%); ^{1}H NMR (500 MHz, DMSO-d_6) δH 8.15 (s, 1H), 7.56 (s, 2H), 6.02 (d, *J* = 2.7 Hz, 1H), 5.66 (dd, *J* = 6.2, 2.7 Hz, 1H), 5.12 (dd, *J* = 6.3, 5.5 Hz, 1H), 5.03 (dd, *J* = 6.2, 3.0 Hz, 1H), 4.16 (td, *J* = 5.8, 3.0 Hz, 1H), 3.52 (dt, *J* = 11.5, 5.5 Hz, 1H), 3.43 (dt, *J* = 11.5, 6.3 Hz, 1H), 1.55 (s, 3H), 1.33 (s, 3H); ^{13}C NMR (126 MHz, DMSO-d_6) δC 154.1, 151.6, 149.6, 126.9, 119.3, 113.3, 91.0, 87.3, 82.0, 81.6, 61.4, 27.1, 25.3; HRMS (ESI) $C_{13}H_{17}N_5O_4{}^{79}Br$ (M + H$^+$) requires 386.0458, found 386.0456; t_R (LCMS) = 1.22 min; IR (FTIR-ATR)/cm^{-1} = 3321, 3172, 2953, 2851, 1657, 1596, 1575, 1497, 1461.

((3aR,4R,6R,6aR)-6-(6-amino-8-((4-chlorobenzyl)amino)-9H-purin-9-yl)-2,2-dimethyltetrahydrofuro[3,4-d][1,3]dioxol-4-yl)-methanol **12**. ((3*aR*,4*R*,6*R*,6*aR*)-6-(6-amino-8-bromo-9*H*-purin-9-yl)-2,2-dimethyltetrahydrofuro[3,4-*d*][1,3]dioxol-4-yl)methanol **11** (1.71 g, 4.44 mmol) and 4-chlorobenzylamine (5.03 g, 35.5 mmol) were dissolved in EtOH (15 mL), and the reaction was heated in microwave for 1 h at 160 °C. The solvent was removed under reduced pressure, and the resulting residue was taken up in EtOAc (50 mL), washed with 1% AcOH solution (3 × 50 mL) and sat. aq. $NaHCO_3$ solution (3 × 50 mL), dried over $MgSO_4$. The solvent was removed under reduced pressure, and the crude product was purified by silica gel chromatography with the Biotage SP1 purification system (EtOAc/EtOH 100:0 to 70:30) to give the title compound **12** as an orange solid (1.93 g, 97%); ^{1}H NMR (500 MHz, DMSO-d_6) δH 7.93 (s, 1H), 7.61 (t, *J* = 6.0 Hz, 1H), 7.40 (d, *J* = 8.8 Hz, 2H), 7.38 (d, *J* = 8.8 Hz, 2H), 6.57 (s, 2H), 6.09 (d, *J* = 3.5 Hz, 1H), 5.47 (dd, *J* = 6.2, 3.5 Hz, 1H), 5.42 (app. t, *J* = 5.2 Hz, 1H), 4.97 (dd, *J* = 6.3, 2.8 Hz, 1H), 4.58 (dd, *J* = 15.6, 5.8 Hz, 1H), 4.53 (dd, *J* = 15.6, 6.0 Hz, 1H), 4.17 (app. td, *J* = 4.4, 2.8 Hz, 1H), 3.59−3.49 (m, 2H), 1.55 (s, 3H), 1.32 (s, 3H); ^{13}C NMR (126 MHz, DMSO-d_6) δC 153.04, 151.44, 149.69, 149.39, 139.23, 131.75, 129.63, 128.62, 117.45, 113.62, 88.37, 85.86, 81.85, 81.63, 61.82, 45.20, 27.61, 25.73; HRMS (ESI) $C_{20}H_{24}N_6O_4{}^{35}Cl$ (M + H$^+$) requires 447.1542, found 447.1525; t_R (LCMS) = 1.36 min; IR (FTIR-ATR)/cm^{-1} = 3190, 2934, 1645, 1607, 1573, 1491, 1457, 1371, 1326, 1213.

((3aR,4R,6R,6aR)-6-(6-amino-8-((4-chlorobenzyl)amino)-9H-purin-9-yl)-2,2-dimethyltetrahydrofuro[3,4-d][1,3]dioxol-4-yl)-methyl 4-(fluorosulfonyl)benzoate **13**. ((3*aR*,4*R*,6*R*,6*aR*)-6-(6-amino-8-((4-chlorobenzyl)amino)-9*H*-purin-9-yl)-2,2-dimethyltetrahydrofuro[3,4-*d*][1,3]dioxol-4-yl)methanol **12** (0.37 g, 0.82 mmol) was dissolved in DMF (8.2 mL) and cooled to 0 °C. Triethylamine (0.12 g, 1.24 mmol) and 4-(fluorosulfonyl)benzoyl chloride (0.22 g, 0.99 mmol) were added, and the reaction stirred at 0 °C for 4 h. The solvent was removed under reduced pressure, and the subsequent oil was taken up in EtOAc (30 mL), washed with sat. NaCl (3 × 30 mL), and dried over $MgSO_4$. The solvent was removed under reduced pressured to give the crude product, which was purified by silica gel chromatography with the Biotage SP1 purification system (EtOAc/EtOH 100:0 to 80:20) to give the title compound **13** as an orange solid (0.29 g, 56%); ^{1}H NMR (600 MHz, $CDCl_3$) δH 8.11 (s, 1H), 8.05 (d, *J* = 8.5 Hz, 2H), 7.99 (d, *J* = 8.6 Hz, 2H), 7.30 (app. s, 4H), 6.13 (dd, *J* = 6.1, 1.6 Hz, 1H), 5.90 (d, *J* = 1.6 Hz, 1H), 5.18 (dd, *J* = 6.1, 3.1 Hz, 1H), 5.14 (s, 2H), 5.02 (app. t, *J* = 5.7 Hz, 1H), 4.62 (dd, *J* = 14.5, 6.1 Hz, 1H), 4.56−4.49 (m, 3H), 4.39 (dd, *J* = 11.8, 5.8 Hz, 1H), 1.60 (s, 3H), 1.44 (s, 3H); ^{13}C NMR (151 MHz, $CDCl_3$) δC

DOI: 10.1021/acs.jmedchem.9b01709
J. Med. Chem. 2019, 62, 11383−11398

164.02, 152.36, 151.76, 150.14, 149.84, 137.04 (d, J = 25.6 Hz), 136.69, 135.61, 133.73, 130.70, 129.24, 129.05, 128.54, 117.85, 114.44, 89.61, 85.43, 82.52, 81.71, 64.87, 46.59, 27.25, 25.55; ^{19}F NMR (471 MHz, $CDCl_3$) δF 65.68; HRMS (ESI) $C_{27}H_{27}N_6O_7SF^{35}Cl$ ($M + H^+$) requires 633.1329, found 633.1360; t_R (LCMS) = 1.57 min; IR (FTIR-ATR)/cm^{-1} = 3192, 1675, 1600, 1492, 1410, 1270, 1211.

((2R,3S,4R,5R)-5-(6-amino-8-((4-chlorobenzyl)amino)-9H-purin-9-yl)-3,4-dihydroxytetrahydrofuran-2-yl)methyl 4-(fluorosulfonyl)-benzoate ***14***. ((3*aR*,4*R*,6*R*,6*aR*)-6-(6-amino-8-((4-chlorobenzyl)-amino)-9*H*-purin-9-yl)-2,2-dimethyltetrahydrofuro[3,4-*d*][1,3]dioxol-4-yl)methyl 4-(fluorosulfonyl)benzoate **13** (77 mg, 0.12 mmol) was dissolved in a 5:2 mixture of TFA/H_2O (1.4 mL) and stirred at room temperature for 30 min. The solvent was then removed under reduced pressure to give the crude product, which was purified by silica gel chromatography with the Biotage SP1 purification system (EtOAc/EtOH 100:0 to 80:20) to give the title compound **14** as an off-white solid (24 mg, 32%); ^{1}H NMR (500 MHz, DMSO-d_6) δH 8.20 (d, J = 8.6 Hz, 2H), 8.12 (d, J = 8.4 Hz, 2H), 7.81 (s, 1H), 7.49 (app. t, J = 6.0 Hz, 1H), 7.38 (d, J = 8.5 Hz, 2H), 7.33 (d, J = 8.5 Hz, 2H), 6.46 (s, 2H), 5.81 (d, J = 4.0 Hz, 1H), 5.46 (d, J = 5.2 Hz, 1H), 5.33 (d, J = 5.9 Hz, 1H), 5.19 (app. q, J = 5.2 Hz, 1H), 4.70−4.63 (m, 2H), 4.53 (app. d, J = 5.9 Hz, 2H), 4.46 (dd, J = 12.0, 5.0 Hz, 1H), 4.16 (app. td, J = 5.3, 3.2 Hz, 1H); ^{13}C NMR (126 MHz, DMSO-d_6) δC 163.82, 152.50, 151.67, 149.52, 148.78, 138.87, 136.18, 135.21 (d, J = 24.0 Hz), 131.22, 130.75, 129.21, 128.77, 128.04, 117.29, 87.67, 80.52, 70.75, 69.65, 64.78, 44.74; ^{19}F NMR (471 MHz, DMSO-d_6) δF 66.03; HRMS (ESI) $C_{24}H_{23}N_6O_7SF^{35}Cl$ ($M + H^+$) requires 593.1016, found 593.1008; t_R (LCMS) = 1.41 min; IR (FTIR-ATR)/cm^{-1} = 3346, 1726, 1637, 1608, 1573, 1409, 1270, 1210.

((2R,3S,4R,5R)-5-(6-amino-8-((4-chlorobenzyl)amino)-9H-purin-9-yl)-3,4-dihydroxytetrahydrofuran-2-yl)methyl 4-cyanobenzoate ***15***. ((3*aR*,4*R*,6*R*,6*aR*)-6-(6-amino-8-((4-chlorobenzyl)amino)-9*H*-purin-9-yl)-2,2-dimethyltetrahydrofuro[3,4-*d*][1,3]dioxol-4-yl)-methanol **12** (0.11 g, 0.24 mmol) was dissolved in DMF (2.4 mL) and cooled to 0 °C. Triethylamine (36 mg, 0.36 mmol) and 4-cyanobenzoyl chloride (47 mg, 0.28 mmol) were added, and the reaction was stirred at 0 °C for 3 h. The solvent was removed under reduced pressured to give the crude product, which was purified by silica gel chromatography with the Biotage SP1 purification system (EtOAc/EtOH 95:5 to 70:30) to give ((3*aR*,4*R*,6*R*,6*aR*)-6-(6-amino-8-((4-chlorobenzyl)amino)-9*H*-purin-9-yl)-2,2-dimethyltetrahydrofuro[3,4-*d*][1,3]dioxol-4-yl)methyl 4-cyanobenzoate as a yellow oil (45 mg, 33%); ^{1}H NMR (500 MHz, $CDCl_3$) δH 8.11 (s, 1H), 7.93 (d, J = 8.7 Hz, 2H), 7.65 (d, J = 8.8 Hz, 2H), 7.29 (s, 4H), 6.09 (dd, J = 6.2, 1.7 Hz, 1H), 5.91 (d, J = 1.7 Hz, 1H), 5.25 (s, 2H), 5.15 (dd, J = 6.2, 3.2 Hz, 1H), 5.07 (app. t, J = 5.7, 1H), 4.61 (dd, J = 14.6, 6.1 Hz, 1H), 4.56−4.51 (m, 2H), 4.46 (dd, J = 11.9, 4.7 Hz, 1H), 4.36 (dd, J = 11.9, 6.0 Hz, 1H), 1.60 (s, 3H), 1.43 (s, 3H); ^{13}C NMR (126 MHz, $CDCl_3$) δC 164.51, 152.35, 151.79, 150.01, 149.86, 136.69, 133.70, 133.09, 132.28, 130.15, 129.20, 129.03, 117.97, 117.82, 116.84, 114.50, 89.62, 85.22, 82.50, 81.65, 64.61, 46.56, 27.24, 25.55; HRMS (ESI) $C_{28}H_{27}N_7O_5{}^{35}Cl$ ($M + H^+$) requires 576.1757, found 576.1746; t_R (LCMS) = 1.51 min. ((3*aR*,4*R*,6*R*,6*aR*)-6-(6-amino-8-((4-chlorobenzyl)amino)-9*H*-purin-9-yl)-2,2-dimethyltetrahydrofuro[3,4-*d*][1,3]dioxol-4-yl)methyl 4-cyanobenzoate was dissolved in a 5:2 mixture of TFA/H_2O (1.4 mL) and stirred at room temperature for 45 min. The solvent was then removed under reduced pressure to give the crude product, which was purified by silica gel chromatography with the Biotage SP1 purification system (EtOAc/EtOH 95:5 to 65:35) to give the title compound **15** as a yellow oil (16 mg, 48%); ^{1}H NMR (500 MHz, DMSO-d_6) δH 7.93 (d, J = 8.9 Hz, 2H), 7.91 (d, J = 8.9 Hz, 2H), 7.83 (s, 1H), 7.48 (app. t, J = 6.0 Hz, 1H), 7.37 (d, J = 8.6 Hz, 2H), 7.33 (d, J = 8.5 Hz, 2H), 6.49 (br. s, 2H), 5.79 (d, J = 3.9 Hz, 1H), 5.45 (d, J = 5.2 Hz, 1H), 5.31 (d, J = 5.9 Hz, 1H), 5.22 (app. td, J = 5.3, 4.0 Hz, 1H), 4.65 (app. q, J = 5.8 Hz, 1H), 4.61 (dd, J = 12.4, 3.5 Hz, 1H), 4.53 (app. d, J = 5.9 Hz, 2H), 4.42 (dd, J = 12.0, 4.7 Hz, 1H), 4.14 (ddd, J = 6.2, 4.6, 3.2 Hz, 1H); ^{13}C NMR (126 MHz, DMSO-d_6) δC 164.28, 152.50, 151.71, 149.51, 148.78, 138.87, 133.30, 132.64, 131.21, 129.74, 129.19, 128.03, 118.04, 117.29, 115.45, 87.65, 80.46, 70.72, 69.56, 64.32, 44.73; HRMS (ESI) $C_{25}H_{23}N_7O_5{}^{35}Cl$ ($M + H^+$) requires 536.1444, found 536.1418; t_R (LCMS) = 1.32 min; IR (FTIR-ATR)/cm^{-1} = 3364, 6101, 2233, 1720, 1611, 1574, 1480, 1435, 1270.

((2R,3S,4R,5R)-5-(6-amino-9H-purin-9-yl)-3,4-dihydroxytetrahydrofuran-2-yl)methyl 4-(fluorosulfonyl)benzoate ***16***. 2′,3′-*O*-isopropylideneadenosine **10** (0.15 g, 0.49 mmol) was dissolved in DMF (2.5 mL). 4-(Fluorosulfonyl)benzoic acid (0.12 g, 0.59 mmol), triethylamine (99 mg, 0.98 mmol), and HBTU (0.22 g, 0.59 mmol) were added, and the reaction was stirred at room temperature for 2 h. The solvent was then removed under reduced pressure to give an orange oil that was taken up in EtOAc (20 mL), washed with sat. aq. $NaHCO_3$ (2 × 20 mL) and sat. NaCl (2 × 20 mL), and dried over $MgSO_4$. The solvent was removed under reduced pressure, and the crude product was purified by silica gel chromatography with the Biotage SP1 purification system (EtOAc/EtOH 100:0 to 70:30) to give ((3*aR*,4*R*,6*R*,6*aR*)-6-(6-amino-9*H*-purin-9-yl)-2,2-dimethyltetrahydrofuro[3,4-*d*][1,3]dioxol-4-yl)methyl 4-(fluorosulfonyl)benzoate as an orange foam (0.16 g, 66%); ^{1}H NMR (600 MHz, $CDCl_3$) δH 8.30 (s, 1H), 8.17 (d, J = 8.3 Hz, 2H), 8.04 (d, J = 8.6 Hz, 2H), 7.86 (s, 1H), 6.10 (d, J = 1.9 Hz, 1H), 5.70 (br. s, 2H), 5.60 (dd, J = 6.3, 1.9 Hz, 1H), 5.23 (dd, J = 6.3, 3.6 Hz, 1H), 4.69 (dd, J = 11.5, 4.1 Hz, 1H), 4.60 (app. dt, J = 6.3, 3.9 Hz, 1H), 4.55 (dd, J = 11.5, 6.3 Hz, 1H), 1.64 (s, 3H), 1.42 (s, 3H); ^{13}C NMR (151 MHz, $CDCl_3$) δC 164.11, 155.63, 153.31, 149.28, 140.21, 137.03 (d, J = 25.4 Hz), 135.98, 130.89, 128.59, 120.57, 114.93, 91.24, 85.19, 84.17, 81.80, 65.42, 27.34, 25.57; ^{19}F NMR (471 MHz, $CDCl_3$) δF 65.78; HRMS (ESI) $C_{20}H_{21}N_5O_7FS$ ($M + H^+$) requires 494.1140, found 494.1152; t_R (LCMS) = 1.40 min. ((3*aR*,4*R*,6*R*,6*aR*)-6-(6-amino-9*H*-purin-9-yl)-2,2-dimethyltetrahydrofuro[3,4-*d*][1,3]dioxol-4-yl)methyl 4-(fluorosulfonyl)benzoate (60 mg, 0.12 mmol) was dissolved in a 5:2 mixture of TFA/H_2O (1.4 mL) and stirred at room temperature for 1 h. The solvent was then removed under reduced pressure to give the crude product, which was purified by reverse-phase C18 chromatography with the Biotage SP1 purification system (water/MeCN + 1% formic acid, 90:10 to 40:60) to give the title compound **16** as an orange oil (41 mg, 74%); ^{1}H NMR (600 MHz, DMSO-d_6) δH 8.31 (s, 1H), 8.27 (d, J = 8.7 Hz, 2H), 8.25 (d, J = 8.7 Hz, 2H), 8.06 (s, 1H), 7.28 (br. s, 2H), 5.93 (d, J = 4.7 Hz, 1H), 5.59 (d, J = 5.7 Hz, 1H), 5.43 (d, J = 5.5 Hz, 1H), 4.77 (app. q, J = 5.2 Hz, 1H), 4.68 (dd, J = 12.0, 3.6 Hz, 1H), 4.52 (dd, J = 12.0, 5.9 Hz, 1H), 4.47 (app. q, J = 5.3 Hz, 1H), 4.24 (app. td, J = 5.5, 3.6 Hz, 1H); ^{13}C NMR (151 MHz, DMSO-d_6) δC 163.88, 156.07, 152.58, 149.20, 140.12, 136.26, 135.28 (d, J = 24.0), 130.92, 128.89, 119.25, 88.18, 81.18, 72.65, 70.10, 65.27; ^{19}F NMR (471 MHz, DMSO-d_6) δF 65.99; HRMS (ESI) $C_{17}H_{17}N_5O_7FS$ ($M + H^+$) requires 454.0827, found 454.0804; t_R (LCMS) = 1.15 min; IR (FTIR-ATR)/cm^{-1} = 3378, 3095, 1738, 1682, 1608, 1576, 1483, 1407, 1378.

((2R,3S,4R,5R)-5-(6-amino-8-(methylamino)-9H-purin-9-yl)-3,4-dihydroxytetrahydrofuran-2-yl)methyl 4-(fluorosulfonyl)benzoate ***17***. ((3*aR*,4*R*,6*R*,6*aR*)-6-(6-amino-8-bromo-9*H*-purin-9-yl)-2,2-dimethyltetrahydrofuro[3,4-*d*][1,3]dioxol-4-yl)methanol **11** (0.40 g, 1.04 mmol) was dissolved in 33% methylamine in ethanol (5.2 mL) and heated in microwave for 1 h at 160 °C. The solvent was removed under reduced pressure, and the crude product was purified by reverse-phase C18 chromatography with the Biotage SP1 purification system (water/MeCN + 1% formic acid, 90:10 to 40:60) to give ((3*aR*,4*R*,6*R*,6*aR*)-6-(6-amino-8-(methylamino)-9*H*-purin-9-yl)-2,2-dimethyltetrahydrofuro[3,4-*d*][1,3]dioxol-4-yl)methanol as an orange oil (0.27 g, 77%); ^{1}H NMR (500 MHz, $CDCl_3$) δH 8.06 (s, 1H), 6.41 (s, 2H), 6.00 (d, J = 4.2 Hz, 1H), 5.76 (app. s, 1H), 5.14 (dd, J = 6.5, 4.2 Hz, 1H), 5.03 (dd, J = 6.4, 2.7 Hz, 1H), 4.36 (app. q, J = 2.2 Hz, 1H), 3.98 (dd, J = 12.1, 2.2 Hz, 1H), 3.85 (dd, J = 12.1, 2.1 Hz, 1H), 2.95 (app. s, 3H), 1.62 (s, 3H), 1.36 (s, 3H); ^{13}C NMR (126 MHz, $CDCl_3$) δC 152.52, 151.40, 149.30, 147.87, 117.23, 114.85, 90.03, 85.38, 82.67, 80.74, 62.16, 29.72, 27.54, 25.38; HRMS (ESI) $C_{14}H_{21}N_6O_4$ ($M + H^+$) requires 337.1619, found 337.1608; t_R (LCMS) = 0.93 min; IR (FTIR-ATR)/cm^{-1} = 3184, 1612, 1581, 1434, 1472, 1376, 1337, 1285, 1211. ((3*aR*,4*R*,6*R*,6*aR*)-6-(6-amino-8-(methylamino)-9*H*-purin-9-yl)-2,2-dimethyltetrahydrofuro[3,4-*d*]-[1,3]dioxol-4-yl)methanol (65 mg, 0.19 mmol) was dissolved in DMF

DOI: 10.1021/acs.jmedchem.9b01709
J. Med. Chem. 2019, 62, 11383−11398

(1.9 mL). 4-(Fluorosulfonyl)benzoic acid (47 mg, 0.23 mmol), triethylamine (39 mg, 0.39 mmol), and HBTU (88 mg, 0.23 mmol) were added, and the reaction was stirred at room temperature for 5 h. The solvent was then removed under reduced pressure to give an orange oil that was taken up in EtOAc (20 mL), washed with sat. aq. $NaHCO_3$ (2 × 20 mL) and sat. NaCl (2 × 20 mL), and dried over $MgSO_4$. The solvent was removed under reduced pressure, and the crude product was purified by silica gel chromatography with the Biotage SP1 purification system (EtOAc/EtOH 100:0 to 60:40) to give ((3*aR*,4*R*,6*R*,6*aR*)-6-(6-amino-8-(methylamino)-9*H*-purin-9-yl)-2,2-dimethyltetrahydrofuro[3,4-*d*][1,3]dioxol-4-yl)methyl 4-(fluorosulfonyl)benzoate as an orange oil (70% pure by LCMS) that was used without further purification; t_R (LCMS) = 1.32 min. ((3*aR*,4*R*,6*R*,6*aR*)-6-(6-amino-8-(methylamino)-9*H*-purin-9-yl)-2,2-dimethyltetrahydrofuro[3,4-*d*][1,3]dioxol-4-yl)methyl 4-(fluorosulfonyl)benzoate was dissolved in a 5:2 mixture of TFA/H_2O (1.4 mL) and stirred at room temperature for 1 h. The solvent was then removed under reduced pressure to give the crude product, which was purified by reverse-phase C18 chromatography with the Biotage SP1 purification system (water/MeCN + 1% formic acid, 90:10 to 40:60) to give the title compound **17** as an orange oil (11 mg, 40%); ^{1}H NMR (600 MHz, MeOD) δH 8.07 (app. s, 4H), 7.85 (s, 1H), 5.70 (d, J = 3.4 Hz, 1H), 5.38 (dd, J = 5.4, 3.4 Hz, 1H), 4.86−4.83 (obs. m, 1H), 4.80 (dd, J = 12.2, 3.1 Hz, 1H), 4.53 (dd, J = 12.2, 4.0 Hz, 1H), 4.29 (app. dt, J = 6.7, 3.5 Hz, 1H), 2.66 (s, 3H); ^{13}C NMR (151 MHz, MeOD) δC 165.46, 154.87, 153.26, 150.78, 150.18, 137.49, 131.71, 129.62, 90.04, 82.91, 72.77, 71.45, 65.03, 40.43, 29.60; ^{19}F NMR (471 MHz, MeOD) δF 63.73; t_R (LCMS) = 1.07 min.

((2R,3S,4R,5R)-5-(6-amino-8-((quinolin-6-ylmethyl)amino)-9H-purin-9-yl)-3,4-dihydroxytetrahydrofuran-2-yl)methyl 4-(fluorosulfonyl)benzoate ***18***. ((3*aR*,4*R*,6*R*,6*aR*)-6-(6-amino-8-bromo-9*H*-purin-9-yl)-2,2-dimethyltetrahydrofuro[3,4-*d*][1,3]dioxol-4-yl)methanol **11** (0.62 g, 1.61 mmol) was dissolved in EtOH (8.0 mL) and added to quinolin-6-yl methanamine (1.11 g, 7.2 mmol), and the reaction was heated in microwave for 2 h at 160 °C. The solvent was removed under reduced pressure, and the resulting residue was taken up in EtOAc (50 mL) and 1% aq. AcOH (50 mL). The product was extracted with EtOAc (3 × 40 mL); washed with 1% aq. AcOH (3 × 40 mL), sat. aq. NaHCO3 (3 × 40 mL), and sat. NaCl (40 mL); and dried over Na_2SO_4. The solvent was removed under reduced pressure, and the crude product was purified by silica gel chromatography with the Biotage SP1 purification system (EtOAc/EtOH 95:5 to 50:50), followed by reverse-phase C18 chromatography with the Biotage SP1 purification system (water/MeCN + 1% formic acid, 80:20 to 0:100) to give ((3*aR*,4*R*,6*R*,6*aR*)-6-(6-amino-8-((quinolin-6-ylmethyl)-amino)-9*H*-purin-9-yl)-2,2-dimethyltetrahydrofuro[3,4-*d*][1,3]dioxol-4-yl)methanol as a yellow oil (60 mg, 8%); ^{1}H NMR (600 MHz, MeOD) δH 8.80 (dd, J = 4.5, 1.7 Hz, 1H), 8.33 (d, J = 8.2 Hz, 1H), 8.12 (app. s, 1H), 8.01 (s, 1H), 7.91 (app. s, 1H), 7.83 (dd, J = 8.8, 2.0 Hz, 1H), 7.51 (dd, J = 8.3, 4.3 Hz, 1H), 6.23 (d, J = 4.3 Hz, 1H), 5.34 (dd, J = 6.4, 4.3 Hz, 1H), 5.03 (dd, J = 6.3, 2.6 Hz, 1H), 4.86−4.79 (obs. m, 2H), 4.34 (app. q, J = 2.8 Hz, 1H), 3.82 (dd, J = 11.7, 3.0 Hz, 1H), 3.76 (dd, J = 11.7, 2.7 Hz, 1H), 1.63 (s, 3H), 1.37 (s, 3H); ^{13}C NMR (151 MHz, MeOD) δC 153.20, 150.93, 150.69, 149.99, 148.07, 139.18, 138.36, 130.76, 129.30, 126.62, 122.75, 117.92, 115.63, 90.58, 86.56, 83.26, 82.43, 62.80, 46.85, 44.55, 40.42, 27.62, 25.59; HRMS (ESI) $C_{23}H_{26}N_7O_4$ (M + H$^+$) requires 464.2041, found 464.2023; t_R (LCMS) = 0.97 min. ((3*aR*,4*R*,6*R*,6*aR*)-6-(6-amino-8-((quinolin-6-ylmethyl)amino)-9*H*-purin-9-yl)-2,2-dimethyltetrahydrofuro[3,4-*d*]-[1,3]dioxol-4-yl)methanol (0.14 g, 0.30 mmol) was dissolved in DMF (2.9 mL). 4-(Fluorosulfonyl)benzoic acid (72 mg, 0.35 mmol), triethylamine (60 mg, 0.59 mmol), and HBTU (0.13 g, 0.35 mmol) were added, and the reaction was stirred at room temperature for 2 h. The solvent was then removed under reduced pressure to give an orange oil that was taken up in EtOAc (20 mL), washed with sat. aq. $NaHCO_3$ (2 × 20 mL) and sat. NaCl (2 × 20 mL), and dried over $MgSO_4$. The solvent was removed under reduced pressure, and the crude product was purified by silica gel chromatography with the Biotage SP1 purification system (EtOAc/EtOH 100:0 to 60:40) to give ((3*aR*,4*R*,6*R*,6*aR*)-6-(6-amino-8-((quinolin-6-ylmethyl)amino)-9*H*-purin-9-yl)-2,2-dimethyltetrahydrofuro[3,4-*d*][1,3]dioxol-4-yl)-methyl 4-(fluorosulfonyl)benzoate as an orange oil (77 mg, 40%); ^{1}H NMR (600 MHz, $CDCl_3$) δH 8.90 (dd, J = 4.2, 1.7 Hz, 1H), 8.11−8.08 (m, 2H), 8.06 (d, J = 8.6 Hz, 1H), 8.00 (d, J = 8.3 Hz, 2H), 7.93 (d, J = 8.6 Hz, 2H), 7.74 (s, 1H), 7.71 (dd, J = 8.7, 2.0 Hz, 1H), 7.40 (dd, J = 8.3, 4.2 Hz, 1H), 6.13 (dd, J = 6.1, 1.6 Hz, 1H), 5.97 (d, J = 1.6 Hz, 1H), 5.28 (app. t, J = 5.7 Hz, 1H), 5.21 (br. s, 2H), 5.18 (dd, J = 6.2, 2.8 Hz, 1H), 4.85 (dd, J = 14.7, 6.1 Hz, 1H), 4.75 (dd, J = 14.7, 5.2 Hz, 1H), 4.55−4.50 (m, 2H), 4.43−4.37 (m, 1H), 1.58 (s, 3H), 1.43 (s, 3H); ^{13}C NMR (151 MHz, $CDCl_3$) δC 164.00, 152.38, 151.86, 150.71, 150.10, 149.86, 147.92, 136.95 (d, J = 25.6 Hz), 136.56, 135.99, 135.55, 130.64, 130.23, 129.44, 128.46, 128.25, 126.21, 121.67, 117.89, 114.46, 89.60, 85.36, 82.53, 81.68, 64.87, 47.08, 27.23, 25.55; ^{19}F NMR (471 MHz, $CDCl_3$) δF 65.69; HRMS (ESI) $C_{30}H_{29}N_7O_7FS$ (M + H$^+$) requires 650.1828, found 650.1810; t_R (LCMS_extended) = 2.55 min; IR (FTIR-ATR)/cm^{-1} = 3328, 1725, 1635, 1606, 1572, 1503, 1410, 1374, 1329, 1268, 1210. ((3*aR*,4*R*,6*R*,6*aR*)-6-(6-amino-8-((quinolin-6-ylmethyl)amino)-9*H*-purin-9-yl)-2,2-dimethyltetrahydrofuro[3,4-*d*][1,3]dioxol-4-yl)methyl 4-(fluorosulfonyl)benzoate (68 mg, 0.10 mmol) was dissolved in a 5:2 mixture of TFA/H_2O (1.4 mL) and stirred at room temperature for 30 min. The solvent was then removed under reduced pressure to give the crude product, which was purified by reverse-phase C18 chromatography with the Biotage SP1 purification system (water/MeCN + 1% formic acid, 90:10 to 60:40), followed by silica gel chromatography with the Biotage SP1 purification system (EtOAc/EtOH 95:5 to 40:60) to give the title compound **18** as an amorphous yellow solid (7 mg, 11%); ^{1}H NMR (600 MHz, DMSO-d_6) δH 8.84 (dd, J = 4.2, 1.7 Hz, 1H), 8.28 (dd, J = 8.5, 0.9 Hz, 1H), 8.18 (d, J = 8.6 Hz, 2H), 8.10 (d, J = 8.5 Hz, 2H), 7.95 (d, J = 8.6 Hz, 1H), 7.90 (d, J = 0.7 Hz, 1H), 7.82 (s, 1H), 7.78 (dd, J = 8.7, 2.0 Hz, 1H), 7.59 (app. t, J = 6.0 Hz, 1H), 7.48 (dd, J = 8.3, 4.2 Hz, 1H), 6.46 (br. s, 2H), 5.86 (d, J = 4.0 Hz, 1H), 5.47 (d, J = 5.2 Hz, 1H), 5.33 (d, J = 5.8 Hz, 1H), 5.22 (app. q, J = 5.0 Hz, 1H), 4.76 (app. d, J = 5.8 Hz, 2H), 4.70 (dd, J = 12.0, 3.2 Hz, 1H), 4.66 (app. q, J = 5.8 Hz, 1H), 4.47 (dd, J = 12.0, 5.0 Hz, 1H), 4.17 (app. td, J = 5.3, 3.2 Hz, 1H); ^{13}C NMR (151 MHz, DMSO-d_6) δC 163.81, 152.52, 151.78, 150.07, 149.54, 148.78, 147.02, 138.09, 136.13, 135.66, 135.17 (d, J = 24.3 Hz), 130.70, 129.55, 128.79, 128.72, 127.57, 125.60, 121.49, 117.32, 87.72, 80.55, 70.78, 69.65, 64.78, 45.42; ^{19}F NMR (471 MHz, DMSO-d_6) δF 66.03; HRMS (ESI) $C_{27}H_{25}N_7O_7FS$ (M + H$^+$) requires 610.1515, found 610.1499; t_R (LCMS_extended) = 2.04 min; IR (FTIR-ATR)/cm^{-1} = 3324, 1724, 1635, 1608, 1573, 1505, 1409, 1330, 1270, 1210.

■ ASSOCIATED CONTENT

Supporting Information

The Supporting Information is available free of charge at https://pubs.acs.org/doi/10.1021/acs.jmedchem.9b01709.

Covalent FP worked example (XLSX)
SMILES molecular formula strings (CSV)
Computational chemistry methods, worked example of the covalent FP-assay, covalent FP and intact-protein MS figures, and NMR spectra of final compounds (PDF)

■ AUTHOR INFORMATION

Corresponding Author

*E-mail: matthew.cheeseman@icr.ac.uk. Phone: (+44) 208 722 4168.

ORCID

Keith Jones: 0000-0002-9440-4094
Matthew D. Cheeseman: 0000-0003-1121-6985

Author Contributions

J.P. synthesized the compounds and carried out the biochemical analysis. M.C. carried out the ROCS conformational analysis. J.P., K.J., and M.D.C. designed the compounds and interpreted the data. J.P. and M.D.C. designed the covalent FP-assay. J.P.

DOI: 10.1021/acs.jmedchem.9b01709
J. Med. Chem. 2019, 62, 11383−11398

and M.D.C. wrote the manuscript. All authors have given approval to the final version of the manuscript.

Funding

This work was funded by an ICR Chairman's Studentship Award (JP) and Cancer Research UK grants (C309/A8274, C309/A11566).

Notes

The authors declare no competing financial interest.

■ ACKNOWLEDGMENTS

The authors would like to thank Katia Grira, Meirion Richards, Maggie Liu, and Amin Mirza of the Structural Chemistry team for their expertise and assistance.

■ ABBREVIATIONS

MOA, mechanism of action; TCI, targeted covalent inhibitor; E, enzyme/protein; EI, reversible enzyme/protein-inhibitor complex; E-I, irreversible enzyme/protein-inhibitor covalent complex; I, inhibitor/ligand; EI*, precovalent complex; K_i, equilibrium constant; k_{inact}, first-order rate constant for covalent inhibition; $t_{1/2}^{inf}$, theoretical half-life at infinite concentration; K_I, concentration at $k_{inact}/2$; k_{obs}, observed first-order rate constant; k_{off}, dissociation rate constant; k_{on}, association rate constant; %CO, percentage covalent occupancy; percentage total occupancy; HSP72, Heat shock 70 kDa protein 1; KRAS, GTPase KRas; HSF1, Heat shock factor protein 1; NBD, nucleotide-binding domain; K_m, Michaelis–Menten constant; SAR, structure–activity relationship; FP, fluorescence polarization; SF, *p*-sulfonyl fluoride; ROCS, rapid overlay of chemical structures; CSD, Cambridge Structural Database; PI3Kδ, Phosphoinositide 3-kinase delta; S_NAr, substitution nucleophilic aromatic; MMP, molecular matched pair; MS, mass spectrometry; SEM, standard error of the mean; NA, not applicable; ND, not determined; App., apparent; S_AN, substitution associative nucleophilic; F_b, fraction bound; A, anisotropy; mP, millipolarization; WT, wild-type; FO, fractional reversible occupancy; sat., saturated; cyc, cyclohexane; EtOAc, ethyl acetate; AcOH, acetic acid; DMF, dimethylformamide; aq., aqueous; DIPEA, diisopropylethylamine; EtOH, ethanol; MeOH, methanol; MeCN, acetonitrile; HATU, 1-[bis(dimethylamino)methylene]-1*H*-1,2,3-triazolo[4,5-*b*]pyridinium 3-oxid hexafluorophosphate; HBTU, *N*,*N*,*N*′,*N*′-Tetramethyl-*O*-(1*H*-benzotriazol-1-yl)uronium hexafluorophosphate

■ REFERENCES

(1) Baillie, T. A. Targeted covalent inhibitors for drug design. *Angew. Chem., Int. Ed. Engl.* **2016**, *55*, 13408–13421.
(2) Johnson, D. S.; Weerapana, E.; Cravatt, B. F. Strategies for discovering and derisking covalent, irreversible enzyme inhibitors. *Future Med. Chem.* **2010**, *2*, 949–964.
(3) Bauer, R. A. Covalent inhibitors in drug discovery: From accidental discoveries to avoided liabilities and designed therapies. *Drug Discovery Today* **2015**, *20*, 1061–1073.
(4) Engel, J.; Richters, A.; Getlik, M.; Tomassi, S.; Keul, M.; Termathe, M.; Lategahn, J.; Becker, C.; Mayer-Wrangowski, S.; Grütter, C.; Uhlenbrock, N.; Krüll, J.; Schaumann, N.; Eppmann, S.; Kibies, P.; Hoffgaard, F.; Heil, J.; Menninger, S.; Ortiz-Cuaran, S.; Heuckmann, J. M.; Tinnefeld, V.; Zahedi, R. P.; Sos, M. L.; Schultz-Fademrecht, C.; Thomas, R. K.; Kast, S. M.; Rauh, D. Targeting drug resistance in egfr with covalent inhibitors: A structure-based design approach. *J. Med. Chem.* **2015**, *58*, 6844–6863.
(5) Marino, S. M.; Gladyshev, V. N. Cysteine function governs its conservation and degeneration and restricts its utilization on protein surfaces. *J. Mol. Biol.* **2010**, *404*, 902–916.
(6) Jakob, C. G.; Upadhyay, A. K.; Donner, P. L.; Nicholl, E.; Addo, S. N.; Qiu, W.; Ling, C.; Gopalakrishnan, S. M.; Torrent, M.; Cepa, S. P.; Shanley, J.; Shoemaker, A. R.; Sun, C. C.; Vasudevan, A.; Woller, K. R.; Shotwell, J. B.; Shaw, B.; Bian, Z.; Hutti, J. E. Novel modes of inhibition of wild-type isocitrate dehydrogenase 1 (IDH1): Direct covalent modification of his315. *J. Med. Chem.* **2018**, *61*, 6647–6657.
(7) Kharenko, O. A.; Patel, R. G.; Brown, S. D.; Calosing, C.; White, A.; Lakshminarasimhan, D.; Suto, R. K.; Duffy, B. C.; Kitchen, D. B.; McLure, K. G.; Hansen, H. C.; van der Horst, E. H.; Young, P. R. Design and characterization of novel covalent bromodomain and extra-terminal domain (BET) inhibitors targeting a methionine. *J. Med. Chem.* **2018**, *61*, 8202–8211.
(8) Mukherjee, H.; Grimster, N. P. Beyond cysteine: Recent developments in the area of targeted covalent inhibition. *Curr. Opin. Chem. Biol.* **2018**, *44*, 30–38.
(9) Strelow, J. M. A perspective on the kinetics of covalent and irreversible inhibition. *SLAS Discovery* **2017**, *22*, 3–20.
(10) $t_{1/2}^{inf} = \ln 2/k_{inact}$
(11) $K_I = (k_{off} + k_{inact})/k_{on}$, $K_i = k_{off}/k_{on}$ When $k_{off} \gg k_{inact}$ then $k_{off} + k_{inact} = \sim k_{off}$ so $K_I = \sim K_i$ k_{off} = reversible dissociation first order rate constant of the non-covalent complex EI, k_{on} = reversible association second order rate constant of the non-covalent complex EI, k_{inact} = first order rate constant of the covalent complex E-I, K_i = true reversible equilibrium constant of the non-covalent complex EI, K_I = pseudo reversible equilibrium constant of the non-covalent complex EI, determined from $k_{obs} = k_{inact}/2$, k_{obs} = concentration dependent pseudo first order rate constant
(12) De Cesco, S.; Kurian, J.; Dufresne, C.; Mittermaier, A. K.; Moitessier, N. Covalent inhibitors design and discovery. *Eur. J. Med. Chem.* **2017**, *138*, 96–114.
(13) Hansen, R.; Peters, U.; Babbar, A.; Chen, Y.; Feng, J.; Janes, M. R.; Li, L.-S.; Ren, P.; Liu, Y.; Zarrinkar, P. P. The reactivity-driven biochemical mechanism of covalent KRASG12C inhibitors. *Nat. Struct. Mol. Biol.* **2018**, *25*, 454–462.
(14) Janes, M. R.; Zhang, J.; Li, L.-S.; Hansen, R.; Peters, U.; Guo, X.; Chen, Y.; Babbar, A.; Firdaus, S. J.; Darjania, L.; Feng, J.; Chen, J. H.; Li, S.; Li, S.; Long, Y. O.; Thach, C.; Liu, Y.; Zarieh, A.; Ely, T.; Kucharski, J. M.; Kessler, L. V.; Wu, T.; Yu, K.; Wang, Y.; Yao, Y.; Deng, X.; Zarrinkar, P. P.; Brehmer, D.; Dhanak, D.; Lorenzi, M. V.; Hu-Lowe, D.; Patricelli, M. P.; Ren, P.; Liu, Y. Targeting KRAS mutant cancers with a covalent G12C-specific inhibitor. *Cell* **2018**, *172*, 578–589.e17.
(15) Fernández-Fernández, M. R.; Valpuesta, J. HSP70 chaperone: A master player in protein homeostasis [version 1; peer review: 3 approved]. *F1000Research* 2018, *7*. DOI: 10.12688/f1000research.15528.1.
(16) Kumar, S.; Stokes, J.; Singh, U. P.; Scissum Gunn, K.; Acharya, A.; Manne, U.; Mishra, M. Targeting HSP70: A possible therapy for cancer. *Cancer Lett.* **2016**, *374*, 156–166.
(17) Powers, M. V.; Jones, K.; Barillari, C.; Westwood, I.; Montfort, R. L. M. V.; Workman, P. Targeting HSP70: The second potentially druggable heat shock protein and molecular chaperone? *Cell Cycle* **2010**, *9*, 1542–1550.
(18) Williamson, D. S.; Borgognoni, J.; Clay, A.; Daniels, Z.; Dokurno, P.; Drysdale, M. J.; Foloppe, N.; Francis, G. L.; Graham, C. J.; Howes, R.; Macias, A. T.; Murray, J. B.; Parsons, R.; Shaw, T.; Surgenor, A. E.; Terry, L.; Wang, Y.; Wood, M.; Massey, A. J. Novel adenosine-derived inhibitors of 70 kDa heat shock protein, discovered through structure-based design. *J. Med. Chem.* **2009**, *52*, 1510–1513.
(19) Rowlands, M.; McAndrew, C.; Prodromou, C.; Pearl, L.; Kalusa, A.; Jones, K.; Workman, P.; Aherne, W. Detection of the ATPase activity of the molecular chaperones HSP90 and HSP72 using the transcreener ADP assay kit. *J. Biomol. Screening* **2010**, *15*, 279–286.
(20) Pettinger, J.; Le Bihan, Y.-V.; Widya, M.; van Montfort, R. L. M.; Jones, K.; Cheeseman, M. D. An irreversible inhibitor of HSP72 that

DOI: 10.1021/acs.jmedchem.9b01709
J. Med. Chem. 2019, 62, 11383–11398

unexpectedly targets lysine-56. *Angew. Chem., Int. Ed. Engl.* **2017**, *56*, 3536−3540.
(21) Pettinger, J.; Jones, K.; Cheeseman, M. D. Lysine-targeting covalent inhibitors. *Angew. Chem., Int. Ed. Engl.* **2017**, *56*, 15200−15209.
(22) Hacker, S. M.; Backus, K. M.; Lazear, M. R.; Forli, S.; Correia, B. E.; Cravatt, B. F. Global profiling of lysine reactivity and ligandability in the human proteome. *Nat. Chem.* **2017**, *9*, 1181.
(23) Cheeseman, M. D.; Westwood, I. M.; Barbeau, O.; Rowlands, M.; Dobson, S.; Jones, A. M.; Jeganathan, F.; Burke, R.; Kadi, N.; Workman, P.; Collins, I.; van Montfort, R. L. M.; Jones, K. Exploiting protein conformational change to optimize adenosine-derived inhibitors of HSP70. *J. Med. Chem.* **2016**, *59*, 4625−4636.
(24) Jones, A. M.; Westwood, I. M.; Osborne, J. D.; Matthews, T. P.; Cheeseman, M. D.; Rowlands, M. G.; Jeganathan, F.; Burke, R.; Lee, D.; Kadi, N.; Liu, M.; Richards, M.; McAndrew, C.; Yahya, N.; Dobson, S. E.; Jones, K.; Workman, P.; Collins, I.; van Montfort, R. L. M. A fragment-based approach applied to a highly flexible target: Insights and challenges towards the inhibition of HSP70 isoforms. *Sci. Rep.* **2016**, *6*, No. 34701.
(25) Vogt, A. D.; Di Cera, E. Conformational selection or induced fit? A critical appraisal of the kinetic mechanism. *Biochemistry* **2012**, *51*, 5894−5902.
(26) Schlecht, R.; Scholz, S. R.; Dahmen, H.; Wegener, A.; Sirrenberg, C.; Musil, D.; Bomke, J.; Eggenweiler, H.-M.; Mayer, M. P.; Bukau, B. Functional analysis of HSP70 inhibitors. *PLoS One* **2013**, *8*, No. e78443.
(27) Xinyi, H. Fluorescence polarization competition assay: The range of resolvable inhibitor potency is limited by the affinity of the fluorescent ligand. *J. Biomol. Screening* **2003**, *8*, 34−38.
(28) $pK_i = -\log K_i\ (M)$.
(29) Kumar, A.; Zhang, K. Y. J. Advances in the development of shape similarity methods and their application in drug discovery. *Front. Chem.* **2018**, *6*, 315.
(30) The Cambridge Structural Database (CSD). https://www.ccdc.cam.ac.uk/solutions/csd-system/components/csd/ (accessed July, 2019).
(31) Martin, J. S.; MacKenzie, C. J.; Fletcher, D.; Gilbert, I. H. Characterising covalent warhead reactivity. *Bioorg. Med. Chem.* **2019**, *27*, 2066−2074.
(32) Dalton, S. E.; Dittus, L.; Thomas, D. A.; Convery, M. A.; Nunes, J.; Bush, J. T.; Evans, J. P.; Werner, T.; Bantscheff, M.; Murphy, J. A.; Campos, S. Selectively targeting the kinome-conserved lysine of PI3Kδ as a general approach to covalent kinase inhibition. *J. Am. Chem. Soc.* **2018**, *140*, 932−939.
(33) Light, S. H.; Minasov, G.; Duban, M.-E.; Anderson, W. F. Adherence to Burgi-Dunitz stereochemical principles requires significant structural rearrangements in Schiff-base formation: Insights from transaldolase complexes. *Acta Crystallogr., Sect. D: Struct. Biol.* **2014**, *70*, 544−552.
(34) Devaraj, N. K.; Perrin, C. L. Approach control. Stereoelectronic origin of geometric constraints on n-to-s and n-to-o acyl shifts in peptides. *Chemical Science* **2018**, *9*, 1789−1794.
(35) Abdul Fattah, T.; Saeed, A.; Albericio, F. Recent advances towards sulfur (vi) fluoride exchange (SUFEX) click chemistry. *J. Fluorine Chem.* **2018**, *213*, 87−112.
(36) Narayanan, A.; Jones, L. H. Sulfonyl fluorides as privileged warheads in chemical biology. *Chem. Sci.* **2015**, *6*, 2650−2659.
(37) Mukherjee, H.; Debreczeni, J.; Breed, J.; Tentarelli, S.; Aquila, B.; Dowling, J. E.; Whitty, A.; Grimster, N. P. A study of the reactivity of S(VI)−F containing warheads with nucleophilic amino-acid side chains under physiological conditions. *Org. Biomol. Chem.* **2017**, *15*, 9685−9695.
(38) Ciuffarin, E.; Senatore, L.; Isola, M. Nucleophilic substitution at four-co-ordinate sulphur. Mobility of the leaving group. *J. Chem. Soc., Perkin Trans. 2* **1972**, 468−471.
(39) Schwartz, P. A.; Kuzmic, P.; Solowiej, J.; Bergqvist, S.; Bolanos, B.; Almaden, C.; Nagata, A.; Ryan, K.; Feng, J.; Dalvie, D.; Kath, J. C.; Xu, M.; Wani, R.; Murray, B. W. Covalent EGFR inhibitor analysis reveals importance of reversible interactions to potency and mechanisms of drug resistance. *Proc. Natl. Acad. Sci. U.S.A.* **2014**, *111*, 173.
(40) Arithmetic mean ± SEM measured from 3 independent biological repeats.
(41) Evans, L. E.; Jones, K.; Cheeseman, M. D. Targeting secondary protein complexes in drug discovery: Studying the druggability and chemical biology of the HSP70/BAG1 complex. *Chem. Commun.* **2017**, *53*, 5167−5170.
(42) Macias, A. T.; Williamson, D. S.; Allen, N.; Borgognoni, J.; Clay, A.; Daniels, Z.; Dokurno, P.; Drysdale, M. J.; Francis, G. L.; Graham, C. J.; Howes, R.; Matassova, N.; Murray, J. B.; Parsons, R.; Shaw, T.; Surgenor, A. E.; Terry, L.; Wang, Y.; Wood, M.; Massey, A. J. Adenosine-derived inhibitors of 78 kda glucose regulated protein (GRP78) ATPase: Insights into isoform selectivity. *J. Med. Chem.* **2011**, *54*, 4034−4041.

DOI: 10.1021/acs.jmedchem.9b01709
J. Med. Chem. 2019, 62, 11383−11398